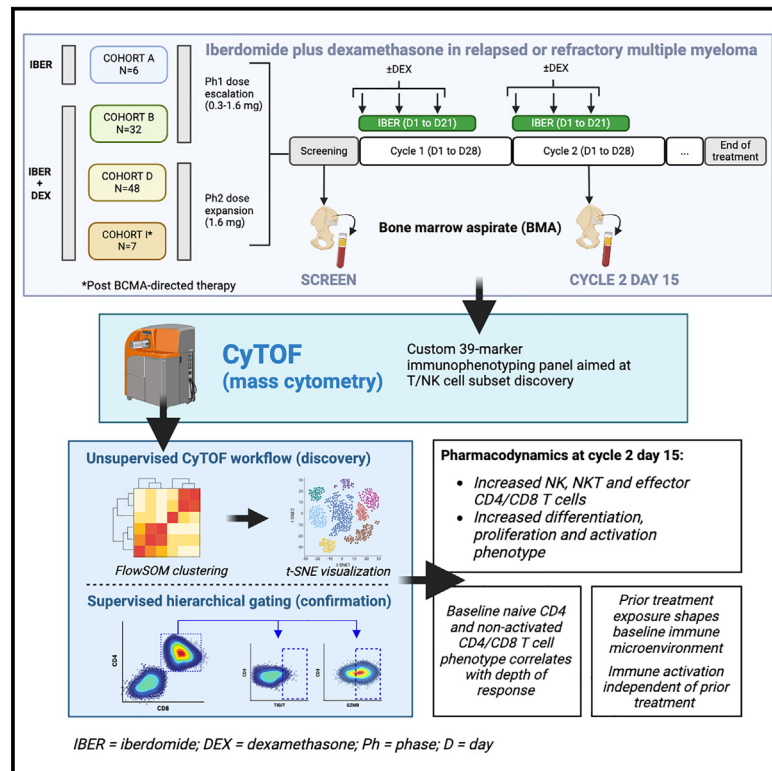# Iberdomide increases innate and adaptive immune cell subsets in the bone marrow of patients with relapsed/refractory multiple myeloma

Graphical abstract

Authors

Oliver Van Oekelen, Michael Amatangelo, Manman Guo, ..., Udo Oppermann, Anjan Thakurta, Samir Parekh

Correspondence

samir.parekh@mssm.edu

In brief

Iberdomide, a CELMoD agent with activity against relapsed/refractory multiple myeloma, increases innate and adaptive immune cell populations in the bone marrow. Employing advanced immunophenotyping, Van Oekelen et al. demonstrate iberdomide's ability to activate T and NK cells in the bone marrow, associated with response to and independent of prior treatment.

Highlights

- Iberdomide treatment boosts innate and adaptive immune cells in human bone marrow

- Activated T and NK cells increase across a population of patients with multiple myeloma

- Changes are independent of treatment exposure/refractoriness and associated with response

- A standardized mass cytometry workflow for immunophenotyping of patient samples

CellPress

Cell Reports Medicine

CellPress
OPEN ACCESS

Article

Iberdomide increases innate and adaptive immune cell subsets in the bone marrow of patients with relapsed/refractory multiple myeloma

Oliver Van Oekelen,[1,2,3] Michael Amatangelo,[4] Manman Guo,[5] Bhaskar Upadhyaya,[3,6] Adam P. Cribbs,[7] Geoffrey Kelly,[8] Manishkumar Patel,[8] Seunghee Kim-Schulze,[3,8] Erin Flynt,[4] Alessandro Lagana,[3,9] Sarah Gooding,[7] Miriam Merad,[3,8,9,11] Sundar Jagganath,[3,6] William E. Pierceall,[4] Udo Oppermann,[5,10] Anjan Thakurta,[4,10] and Samir Parekh[3,6,9,11,12,*]

[1]Department of Medicine, Mount Sinai Beth Israel, Icahn School of Medicine at Mount Sinai, New York, NY, USA
[2]Department of Genetics and Genomic Sciences, Icahn School of Medicine at Mount Sinai, New York, NY, USA
[3]Tisch Cancer Institute, Icahn School of Medicine at Mount Sinai, New York, NY, USA
[4]Translational Medicine, Bristol Myers Squibb, Summit, NJ, USA
[5]Nuffield Department of Orthopaedics, Rheumatology and Musculoskeletal Sciences, Oxford University, Oxford, UK
[6]Department of Medicine, Hematology and Medical Oncology, Icahn School of Medicine at Mount Sinai, New York, NY, USA
[7]MRC Molecular Haematology Unit, Weatherall Institute of Molecular Medicine, University of Oxford, Oxford, UK
[8]Human Immune Monitoring Center, Icahn School of Medicine at Mount Sinai, New York, NY, USA
[9]Department of Oncological Sciences, Icahn School of Medicine at Mount Sinai, New York, NY, USA
[10]Oxford Translational Myeloma Centre (OTMC), Nuffield Department of Orthopaedics, Rheumatology and Musculoskeletal Sciences, University of Oxford, Oxford, UK
[11]Precision Immunology Institute, Icahn School of Medicine at Mount Sinai, New York, NY, USA
[12]Lead contact
*Correspondence: samir.parekh@mssm.edu
https://doi.org/10.1016/j.xcrm.2024.101584

SUMMARY

Iberdomide is a potent cereblon E3 ligase modulator (CELMoD agent) with promising efficacy and safety as a monotherapy or in combination with other therapies in patients with relapsed/refractory multiple myeloma (RRMM). Using a custom mass cytometry panel designed for large-scale immunophenotyping of the bone marrow tumor microenvironment (TME), we demonstrate significant increases of effector T and natural killer (NK) cells in a cohort of 93 patients with multiple myeloma (MM) treated with iberdomide, correlating findings to disease characteristics, prior therapy, and a peripheral blood immune phenotype. Notably, changes are dose dependent, associated with objective response, and independent of prior refractoriness to MM therapies. This suggests that iberdomide broadly induces innate and adaptive immune activation in the TME, contributing to its antitumor efficacy. Our approach establishes a strategy to study treatment-induced changes in the TME of patients with MM and, more broadly, patients with cancer and establishes rational combination strategies for iberdomide with immune-enhancing therapies to treat MM.

INTRODUCTION

Immunomodulatory agents (IMiDs; e.g., lenalidomide, pomalidomide) have played a critical role in improving outcomes for patients with multiple myeloma (MM).[1–5] These agents modulate cereblon (CRBN), the substrate receptor of the CUL4A/DDB1/Roc1 E3 ligase complex, to induce polyubiquitination and subsequent degradation of substrate proteins, including the key hematopoietic transcription factors Ikaros (IKZF1) and Aiolos (IKZF3).[6,7] Ikaros and Aiolos are required for growth and promote the survival of lymphocytes, including B and plasma cells, and their loss in myeloma cells results in direct antiproliferative effects via the downregulation of c-Myc and IRF4.[7–16]

Ikaros and Aiolos also regulate immune cell development and homeostasis, and their downregulation induces multiple effects on T, B, and natural killer (NK) cells.[11,15,17] Consequently,

in vitro studies with lenalidomide and pomalidomide have demonstrated co-stimulatory effects in primary human T and NK cells from peripheral blood.[7,17–21] In clinical studies, an increase in bone marrow T cells was observed in patients receiving lenalidomide therapy.[22,23] Similarly, pomalidomide treatment was associated with innate and adaptive immunity correlating with antitumor efficacy.[24,25] T and NK cell changes are also largely consistent among patients treated with pomalidomide in triplet combinations with dexamethasone and cyclophosphamide or daratumumab.[26–28] However, the bone marrow immune microenvironment composition of patients refractory to IMiDs and the potential for immune activation with subsequent therapy after relapse are largely unknown and of great importance given the ongoing development of immune-mediated therapies for patients with relapsed/refractory MM (RRMM) with prior exposure to these agents.
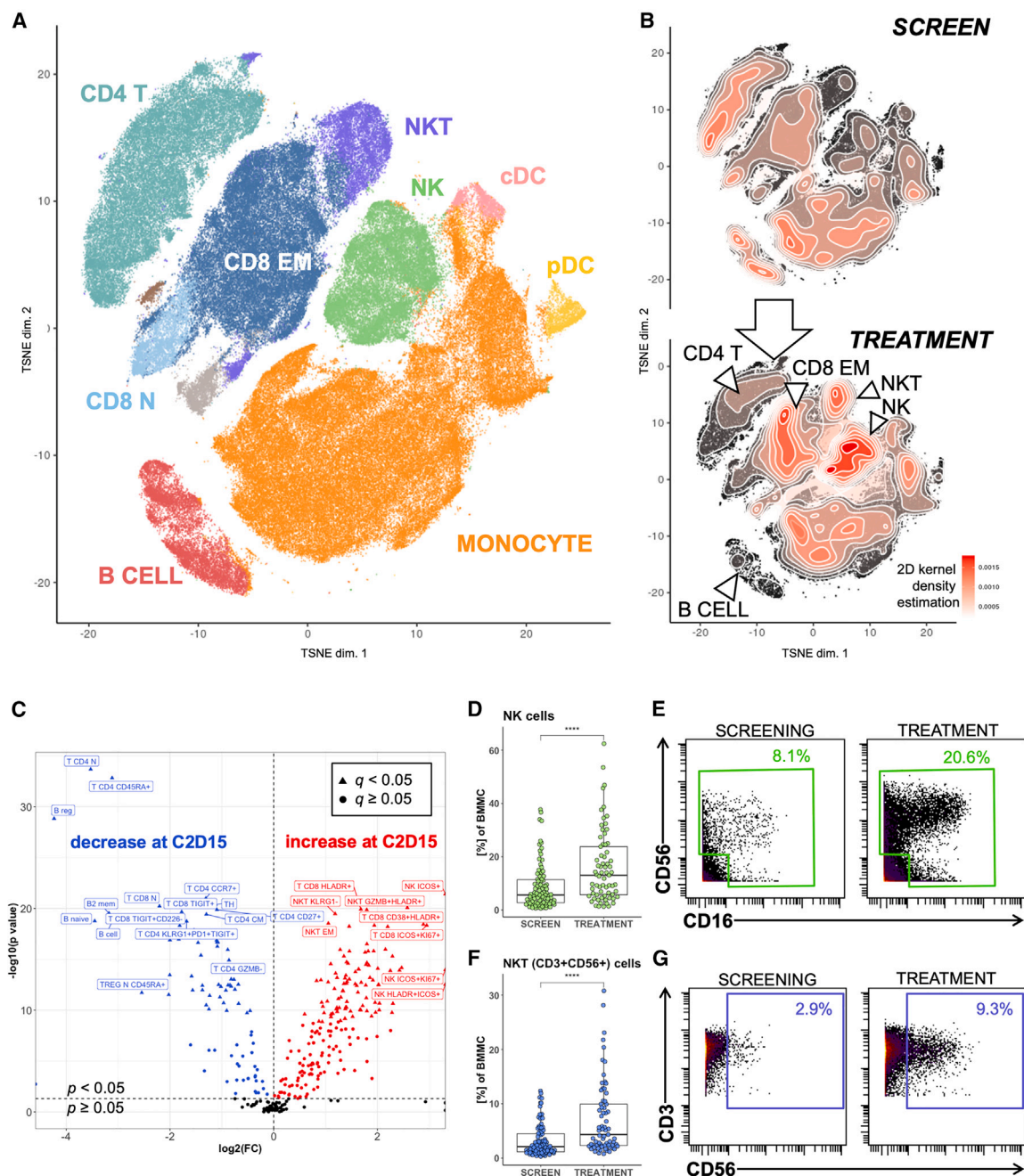
Figure 1. Mid-cycle 2 changes (C2D15) of the immune phenotype following iberdomide treatment show activation/proliferation of T, NK, and NKT cells

(A) t-Distributed stochastic neighbor embedding (t-SNE) representation of the bone marrow mononuclear cells (BMMCs) of all (*n* = 93) patients included in the analysis at both time points. The cells were clustered using a FlowSOM-based clustering strategy, and clusters were manually annotated based on the expression of canonical markers. While all cells were included in the clustering analysis, a subset of 1,000 cells were randomly selected for inclusion in the t-SNE plot.

(B) t-SNE plot of BMMCs of all (*n* = 93) patients included in the analysis at both time points, split between cells collected before treatment with iberdomide ± dexamethasone (screen, top) and at the cycle 2 day 15 (C2D15) time point (treatment, bottom). Individual cells are shown as black dots. A random sample of 1,000 cells per sample was selected for inclusion in the plot. The overlaying heatmap in red corresponds to a 2D kernel density estimation showing the abundance of cell populations on the t-SNE plot, where areas in bright red correspond to a high local abundance of cells.

(C) Volcano plot showing proportion changes of the various immune cell populations that were identified using the manual gating approach. Shown is log2 fold change of relative abundance within the BMMC population at the C2D15 time point vs. screening time point vs. log10 of the *p* value of a Mann-Whitney U test comparing both time points. Populations that were significant after correction using the Benjamini-Hochberg approach are shown as triangles. Some of the most significant populations are labeled on the plot.

(legend continued on next page)

Cell Reports Medicine
Article

CellPress
OPEN ACCESS

Iberdomide is a potent CRBN E3 ligase modulator (CELMoD agent) with structural similarities to lenalidomide and pomalidomide. Notably, iberdomide binds CRBN with a 20-fold higher affinity and induces allosteric rearrangement in CRBN, leading to more efficient substrate recruitment and degradation of Ikaros and Aiolos, compared to lenalidomide or pomalidomide.[29,30] In preclinical models, iberdomide has been shown to enhance immune co-stimulatory activities when compared to lenalidomide or pomalidomide, including increased interleukin-2 secretion and granzyme B (GZMB) degranulation in stimulated peripheral blood mononuclear cells and enhanced immune-mediated killing of myeloma cells.[31,32] Furthermore, iberdomide increases the activity of daratumumab more potently than other immunomodulatory compounds and enhances the activity of B-cell maturation antigen (BCMA)-targeted chimeric antigen receptor (CAR) T cell-based therapies *in vitro*.[33–35]

Iberdomide has shown clinical activity with durable responses in a large phase 1/2 study for patients with heavily pretreated RRMM, including those with triple-class refractory disease.[36] This work provides important insights into the immune tumor microenvironment of patients enrolled in this study and the pharmacodynamic effects of iberdomide in this population, including patients exposed or refractory to lenalidomide, pomalidomide, anti-CD38 monoclonal antibody (mAb), and/or BCMA-targeted therapies. Whereas previous studies have focused mainly on preclinical data or studied the immune effects of immunomodulatory and CELMoD agents in the peripheral blood, here, we present a large-scale characterization of the bone marrow immune microenvironment. We developed and used a large-scale mass cytometry panel to directly capture tumor microenvironment immune dynamics in the largest study of patients with RRMM to date.

RESULTS

Iberdomide induces expansion of NK and NKT cells in RRMM bone marrow microenvironment

We compared baseline and on-treatment (cycle 2 day 15) bone marrow mononuclear cells (BMMCs) by mass cytometry (CyTOF) using a panel of 39 markers. This approach allowed the determination of the relative abundance of immune subpopulations in great detail (Figures 1A and S1). The panel consists of general lineage markers for the major immune cell types present in the microenvironment, as well as an extensive set of markers associated with T and NK cell differentiation, activation, or exhaustion. A predefined hierarchical supervised gating strategy was employed and compared with unsupervised gating (STAR Methods; Figure S2) to reduce potential bias. Compared with baseline, iberdomide treatment resulted in major shifts of the relative immune compositions at the cycle 2 day 15 (mid-cycle

2) time point in the bone marrow tumor microenvironment. The unsupervised analysis suggested a relative increase in NK cells, natural killer T (NKT; i.e., $CD3^+CD56^+$) cells, and effector memory (EM) $CD8^+$ T cells, with a decrease of B and $CD4^+$ T cells, as shown by the overlay of density on the t-distributed stochastic neighbor embedding (t-SNE) plot (Figure 1B). The shift in these same populations was confirmed using a hierarchical gating approach (Figures 1C and S3). Specifically, we noted a significant expansion of NK cells (median 5.6% vs. 13.1% of BMMCs, $p < 0.001$) (Figures 1D and 1E) and NKT cells (median 2.2% vs. 4.3% of BMMCs, $p < 0.001$) (Figures 1F and 1G), whereas B cells (median 4.0% vs. 0.5% of BMMCs, $p < 0.001$), $CD4^+$ T cells (median 16.4% vs. 7.8% of BMMCs, $p < 0.001$), monocytes (median 21.6% vs. 16.3% of BMMCs, $p < 0.001$), and conventional dendritic cells (DCs) (median 5.3% vs. 3.9% of BMMCs, $p < 0.001$) decreased (Figure S3). We found no significant change in the relative proportion of overall $CD3^+$ T cells, $CD8^+$ T cells, or plasmacytoid DCs. The direction of observed changes was consistent when limiting the analysis to the subgroup of 6 patients treated with iberdomide monotherapy (i.e., without dexamethasone), but the changes were not statistically significant (Figure S4). The NKT cell increase was largely limited to the expansion of $CD8^+$ NKT cells (median 1.3% vs. 3.3% of BMMCs, $p < 0.001$), whereas $CD4^+$ NKT cell frequency was stable (Figure S5).

T cell subsets in the tumor microenvironment shift toward effector differentiation, increased proliferation, and co-stimulatory receptor/immune checkpoint expression, suggesting activation

While the overall T cell percentages remained stable, T cell subpopulations showed distinct subpopulation shifts toward a functionally activated phenotype, which was initially noted as a shift in the density overlay of the t-SNE plot of the subset of $CD3^+$ cells (Figures 2A and 2B). Indeed, for both $CD4^+$ and $CD8^+$ T cells, a significant shift toward an EM phenotype (i.e., $CD45RA^-CCR7^-$) at the mid-cycle 2 time point compared to baseline (median 67.0% vs. 84.2% of $CD8^+$ T cells, $p < 0.001$ [Figure 2C], and 52.0% vs. 67.0% of $CD4^+$ T cells, $p < 0.001$ [Figure S5]) was observed. This change was associated with a concurrent relative decrease of naive ($CD45RA^+CCR7^+$, $p < 0.001$), central memory ($CD45RA^-CCR7^+$, $p < 0.01$), and terminally differentiated EM cells re-expressing CD45RA ($CD45RA^+CCR7^-$, $p < 0.05$) $CD4^+$ and $CD8^+$ T cells (Figure S5). Proliferating $CD4^+$ or $CD8^+$ T and NKT cells were approximated by comparing the Ki-67$^+$ fraction at cycle 2 day 15 vs. baseline in the available paired samples, which showed a significant increase of Ki-67$^+$ $CD8^+$ T cells (Figure 2D) (median 2.0% vs. 7.0% of $CD8^+$ T cells, $p < 0.001$) and Ki-67$^+CD4^+$ T cells (Figure S6A) (median 2.2% vs. 4.7% of $CD4^+$ T cells, $p < 0.001$).

(D and E) Relative abundance of natural killer (NK) cells (D) and natural killer T (NKT) cells (E) as a percentage of BMMCs, shown before treatment with iberdomide ± dexamethasone (screen) and at the C2D15 time point (treatment).

(F and G) Representative bivariate flow cytometry dot plot showing the change in NK (F) or NKT (G) cells as a percentage of BMMCs at screen vs. treatment time points.

In (D) and (F), each dot represents a patient sample. Boxplots show median, Q1 and Q3 quartiles, and whiskers up to 1.5× interquartile range (****$p < 0.0001$, ***$p < 0.001$, **$p < 0.01$, *$p < 0.05$, and ns, $p \geq 0.05$, Mann-Whitney U test). In (E) and (G), each dot represents a single cell.
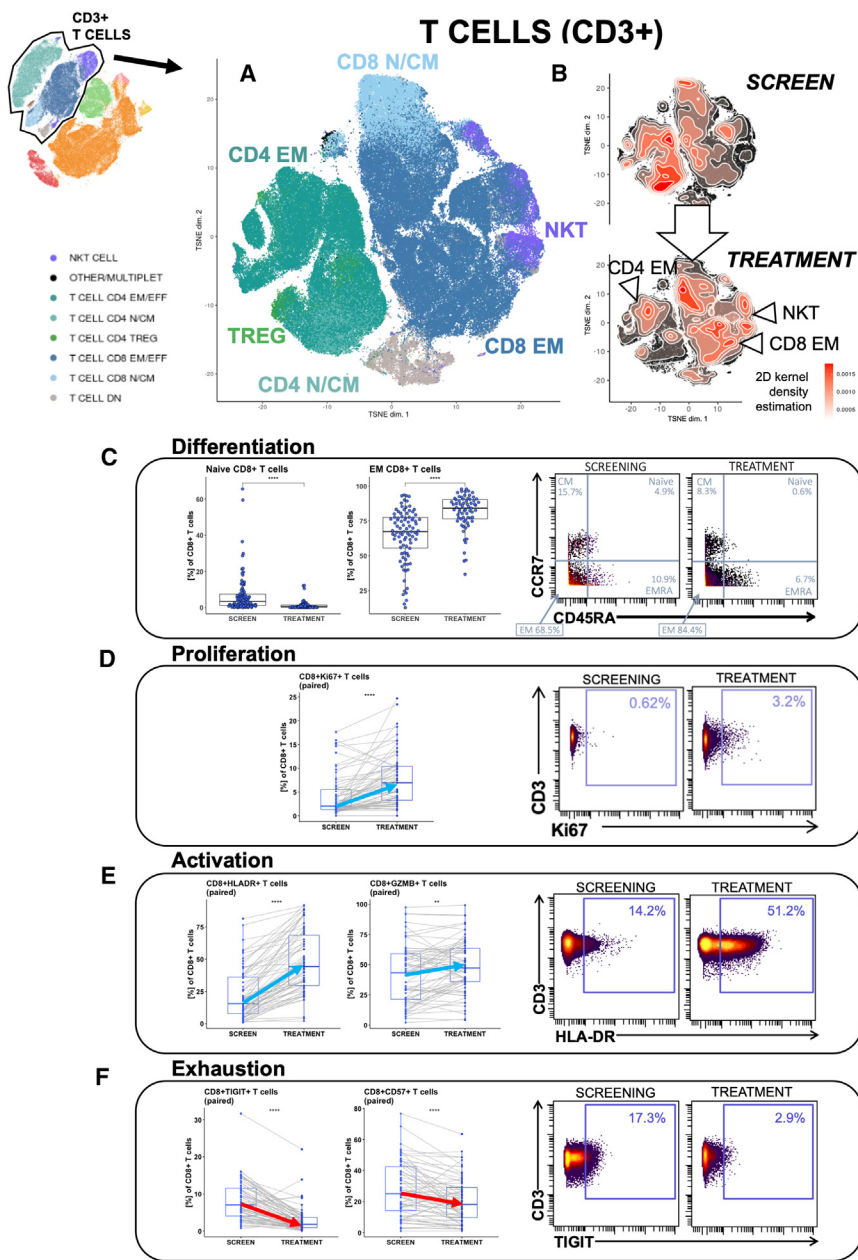
See also Figures S1–S4, S8, S12, and S13.

Figure 2. Mid-cycle 2 changes (C2D15) of the T cell phenotype following iberdomide treatment demonstrate differentiation, proliferation, and activation

(A) t-SNE representation of CD3$^+$ cells (i.e., T cells) of all (n = 93) patients included in the analysis at both time points. The cells were clustered using a FlowSOM-based clustering strategy, and clusters were manually annotated based on the expression of canonical markers. While all cells were included in the clustering analysis, a subset of 1,000 cells were randomly selected for inclusion in the t-SNE plot.

(B) t-SNE plot of T cells of all (n = 93) patients included in the analysis at both time points, split between cells collected before treatment with iberdomide ± dexamethasone (screen, top) and at the C2D15 time point (treatment, bottom). Individual cells are shown as black dots. A random sample of 1,000 cells per sample was selected for inclusion in the plot. The overlaying heatmap in red corresponds to a 2D kernel density estimation showing the abundance of cell populations on the t-SNE plot, where areas in bright red correspond to a high local abundance of cells.

(C) Relative abundances of naive and effector memory (EM) CD8$^+$ T cells as a percentage of all CD8$^+$ T cells (parent population) before treatment with iberdomide ± dexamethasone (screen) and at the C2D15 time point (treatment). T cell differentiation subsets were defined based on the expression of CCR7 and CD45RA and included naive (CCR7$^+$CD45RA$^+$), central memory (CM; CCR7$^+$CD45RA$^-$), EM (CCR7$^-$CD45RA$^-$), and terminally differentiated EM cells re-expressing CD45RA (EMRA; CCR7$^-$CD45RA$^+$). The change between time points is illustrated by a representative dot plot (right) showing the percentage of the parent population gate.

(D) Relative abundances of CD8$^+$ T cells expressing the proliferation marker Ki-67 as a percentage of all CD8$^+$ T cells (parent population) within paired samples, shown before treatment with iberdomide ± dexamethasone (screen) and at the C2D15 time point (treatment). The change between time points is illustrated by a representative dot plot (right) showing the percentage of the parent population gate.

(E) Relative abundances of CD8$^+$ T cells expressing the activation markers HLA-DR and granzyme B (GZMB) as a percentage of all CD8$^+$ T cells (parent population) within paired samples, shown before treatment with iberdomide ± dexamethasone (screen) and at the C2D15 time point (treatment). The change between time points is illustrated by a representative dot plot (right) showing the percentage of the parent population gate.

(F) Relative abundances of CD8$^+$ T cells expressing the exhaustion marker TIGIT and the senescence marker CD57 as a percentage of all CD8$^+$ T cells (parent population) within paired samples, shown before treatment with iberdomide ± dexamethasone (screen) and at the C2D15 time point (treatment). The change between time points is illustrated by a representative dot plot (right) showing the percentage of the parent population gate.

In (C)–(F), each dot on the boxplot represents a patient sample. Arrows illustrate the change in the median proportion. Boxplots show median, Q1 and Q3 quartiles, and whiskers up to 1.5× interquartile range (****p < 0.0001, ***p < 0.001, **p < 0.01, *p < 0.05, and ns, $p \geq$ 0.05, Mann-Whitney U test). On the flow cytometry dot plot, each dot corresponds to a single cell.

See also Figures S5–S7.

We used paired bone marrow samples to study whether iberdomide treatment changed the expression of surface and intracellular markers known to be associated with functional activation and/or exhaustion of T and NK cells *in vivo*. Within the CD4$^+$ T cell and CD8$^+$ T cell population, we observed a significant increase of subsets expressing the following markers,

Cell Reports Medicine
Article
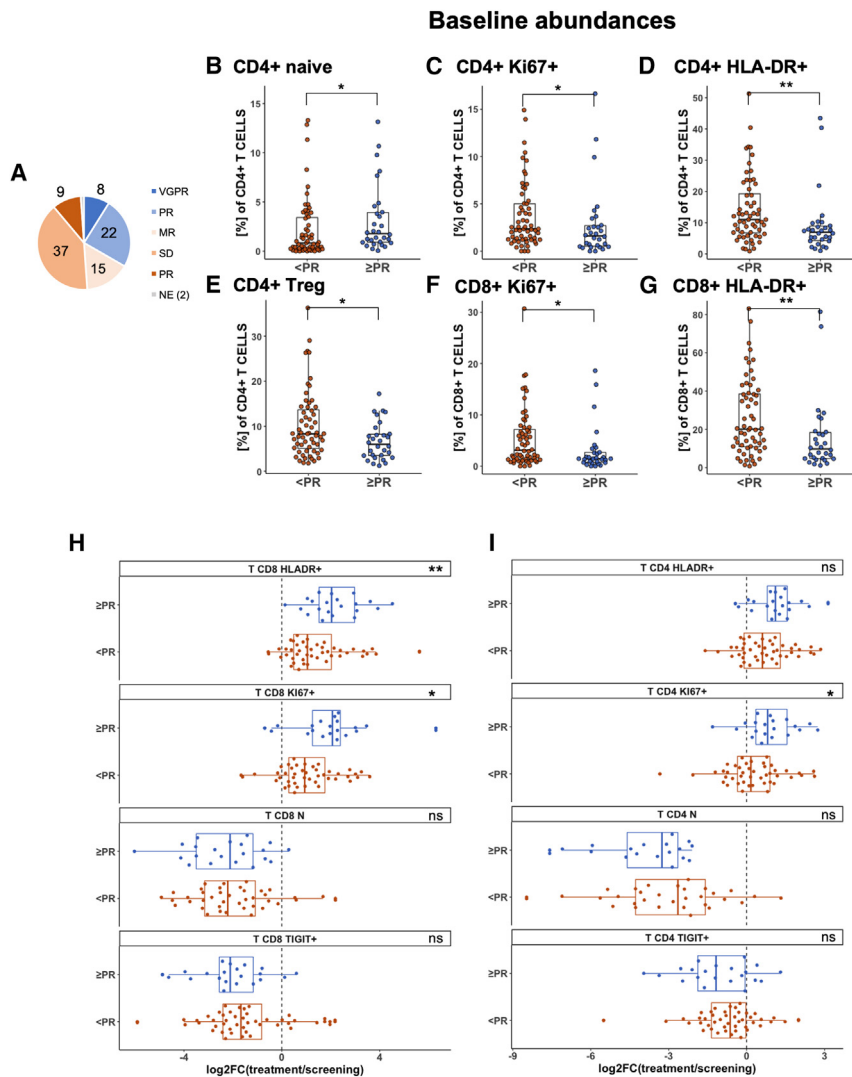
CellPress
OPEN ACCESS

Figure 3. A more naive and inactivated T cell phenotype at baseline is associated with clinical response to iberdomide treatment

(A) Pie chart stratifying all patients ($n = 93$) by response according to International Myeloma Working Group (IMWG) criteria. VGPR, very good partial response; PR, partial response; MR, minor response; SD, stable disease; PD, progressive disease.

(B–G) Relative abundances of selected immune cell populations (naive $CD4^+$ T cells, B; Ki-67$^+$ $CD4^+$ T cells, C; HLA-DR$^+$ $CD4^+$ T cells, D; regulatory T cells, E; Ki-67$^+$ $CD8^+$ T cells, F; and HLA-DR$^+$ $CD8^+$ T cells, G) as a percentage of the parent population (as indicated on the y axis), shown before treatment with iberdomide ± dexamethasone (i.e., screening time point) split by whether patients obtained an objective response (≥PR, $n = 30$) vs. did not obtain an objective response (<PR, $n = 61$). For 2 patients, no response data were available (NE).

(H and I) Log2 fold change of C2D15 (treatment) time point vs. screening time point of selected immune cell populations, split by whether patients obtained an objective response (≥PR, $n = 30$) vs. did not obtain an objective response (<PR, $n = 61$). In (B)–(H), each dot on the boxplot represents a patient sample. Boxplots show median, Q1 and Q3 quartiles, and whiskers up to 1.5× interquartile range (****$p < 0.0001$, ***$p < 0.001$, **$p < 0.01$, *$p < 0.05$, and ns, $p \geq 0.05$, Mann-Whitney U test).

inhibitory checkpoints (e.g., KLRG1$^+$PD-1$^+$TIGIT$^+$) significantly decreased (median 2.0% vs. 0.6% of $CD8^+$ T cells, $p < 0.001$) (Figure S6C). Similar trends were noted for the $CD4^+$ T cell subpopulations (Figure S7).

The major pharmacodynamic changes (i.e., relative increase of NK cells and HLA-DR$^+$ or Ki-67$^+$ $CD8^+$ T cells; relative decrease of B cells, monocytes, and TIGIT$^+$ or KLRG1$^+$ $CD8^+$ T cells) showed a dose-dependent effect, supporting a causal model of iberdomide treatment resulting in the observed changes (Figure S8).

Baseline T cell phenotype of naive, non-activated T cells and lower regulatory T cells correlates with objective response

We investigated whether relative abundances at the screening time point or dynamic changes were associated with objective response. Therefore, we compared the 30 patients who achieved an objective response by the 2016 International Myeloma Working Group criteria (i.e., partial response [PR] or better) to the other patients (Figure 3A). Manual gating confirmed that a significantly higher abundance of naive $CD4^+$ T cells (Figure 3B, $p < 0.05$) and a lower abundance of Ki-67$^+$ (Figures 3C–3F, $p < 0.05$) and HLA-DR$^+$ (Figures 3D–3G, $p < 0.01$) $CD4^+$ and $CD8^+$ T cells at the screening time point were associated with objective response. Furthermore, the relative abundance of

suggesting a more activated and cytotoxic phenotype: CD28 (median 69.8% vs. 76.5% of $CD4^+$ T cells, $p < 0.001$; median 21.9% vs. 23.1% of $CD8^+$ T cells, $p < 0.001$), CD38 (median 13.2% vs. 22.9% of $CD4^+$ T cells, $p < 0.001$; median 17.2% vs. 40.7% of $CD8^+$ T cells, $p < 0.001$), ICOS (median 3.8% vs. 11.8% of $CD4^+$ T cells, $p < 0.001$; median 0.8% vs. 2.0% of $CD8^+$ T cells, $p < 0.001$), GZMB (median 43.1% vs. 47.2% of $CD8^+$ T cells, $p < 0.01$), and HLA-DR (median 9.1% vs. 29.5% of $CD4^+$ T cells, $p < 0.001$; median 15.5% vs. 44.4% of $CD8^+$ T cells, $p < 0.001$) (Figures 2E and S6B). In contrast, in $CD8^+$ T cells we observed a significant decrease of T cell subsets expressing markers associated with immune exhaustion or terminal differentiation and senescence, including decreases in expression of TIGIT (median 7.0% vs. 1.8% of $CD8^+$ T cells, $p < 0.001$), KLRG1 (median 47.1% vs. 37.6% of $CD8^+$ T cells, $p < 0.001$), and CD57 (median 25.0% vs. 18.2% of $CD8^+$ T cells, $p < 0.001$) (Figures 2F and S6C). While PD-1$^+$$CD8^+$ T cells increased at cycle 2 day 15 (median 23.9% vs. 31.2% of $CD8^+$ T cells, $p < 0.01$), $CD8^+$ T cells co-expressing multiple

regulatory T cells was lower in patients achieving deeper responses (Figure 3E). Moreover, the pharmacodynamic changes in T cell populations associated with iberdomide treatment were larger in those patients that achieved at least PR (Figures 3H and 3I), specifically for HLA-DR$^+$ CD8$^+$ T cells (median fold change [FC] 2.44 in non-responders vs. 4.77 in responders, $p < 0.01$), HLA-DR$^+$ CD4$^+$ T cells (median FC 1.31 vs. 2.11), Ki-67$^+$CD8$^+$ T cells (median FC 1.91 vs. 3.21, $p < 0.05$), and Ki-67$^+$CD4$^+$ T cells (median FC 1.17 vs. 1.97, $p < 0.05$). Conversely, a trend showing more pronounced decreases of naive CD8$^+$ and CD4$^+$ T cells and TIGIT$^+$ CD8$^+$ and CD4$^+$ T cells was noted.

NK cell subsets in the tumor microenvironment proliferate, increase, and shift toward an activated phenotype

Within the NK cell population, expansion of both CD56^{bright}CD16$^-$ (cytokine-producing) NK cells (median 2.8% vs. 7.1% of BMMCs, $p < 0.001$) and in CD56^{dim}CD16$^+$ (cytotoxic) NK cells (median 1.6% vs. 2.9% of BMMCs, $p < 0.01$) was observed at cycle 2 day 15 (Figures 4A–4C). Furthermore, we observed a significant increase in NK cell proliferation markers: Ki-67$^+$ NK cells (median 6.3% vs. 9.1% of NK cells, $p < 0.01$) (Figure 4D). We also saw a shift toward an activated and cytotoxic phenotype with an increase of CD38 (median 72.5% vs. 90.4% of NK cells, $p < 0.001$), GZMB (median 39.4% vs. 67.2% of NK cells, $p < 0.001$), and CD57, a marker associated with high cytotoxic potential but reduced proliferative capacity in NK cells (median 12.7% vs. 23.0% of NK cells, $p < 0.001$) (Figures 4E and S9). Conversely, we observed a decrease of TIGIT (median 5.3% vs. 2.2% of NK cells, $p < 0.001$) and KLRG1 (median 8.9% vs. 7.2% of NK cells, $p < 0.01$) (Figures 4F and S9), markers associated with exhaustion. Furthermore, specific to NK cells, there was a relative increase of NK cells expressing the co-stimulatory receptors NKG2D (median 57.5% vs. 62.1% of NK cells, $p < 0.01$) and CD226 (median 17.1% vs. 26.1% of NK cells, $p < 0.001$). However, we also observed an increase of NK cells expressing the co-inhibitory receptor NKG2A (median 39.2% vs. 52.8% of NK cells, $p < 0.001$) (Figure S9).

While prior therapy shapes the microenvironment, T and NK cell activation occurs independent of microenvironment changes with prior therapy in patients with RRMM

To investigate how previous therapies influenced the tumor microenvironment and to understand whether iberdomide could induce the immunostimulatory changes observed above in patients with prior refractoriness to IMiDs, anti-CD38, or BCMA-targeted therapies, we compared these patient subgroups to the whole cohort. We found that the immune microenvironment composition at baseline (i.e., the screening time point) varied strongly based on last prior therapy (Figure 5). Specifically, patients treated with anti-CD38 mAb therapy as the last prior therapy ($n = 27$) showed clear differences compared to all other patients. We observed similar proportions of CD4$^+$ T cells but significantly higher proportions of CD8$^+$ T cells ($p < 0.001$) and significantly lower proportions of NK cells ($p < 0.001$). Within the CD4$^+$ and CD8$^+$ T cell compartment, cells expressing CD38 or HLA-DR were significantly

($p < 0.05$) less abundant in those patients with anti-CD38 mAb treatment immediately prior to study enrollment. Significant phenotypic differences in NK cells were also observed in patients previously treated with anti-CD38 mAb therapy, including a higher abundance of NK cells expressing CD27 ($p < 0.05$) or CD127 ($p < 0.001$) and lower abundance of NK cells expressing CD16, CD38, CD56, CD57, NKG2A, NKG2D, GZMB, and Tbet (all $p < 0.01$), suggesting that prior anti-CD38 mAb therapy decreases NK cells in the bone marrow and, in doing so, leaves behind a more immature subset (Figures 5A and S10). Whereas relative monocyte levels overall were not significantly different, patients immediately after anti-CD38 mAb therapy had lower proportions of CD16$^+$ monocytes ($p < 0.001$). Notably, in the 7 patients who were previously treated with a BCMA-targeted therapy (antibody-drug conjugate or CAR T cell), immune cell population abundance at baseline was not significantly different from the other patients, although there was a trend toward an increased relative abundance of monocytes (Figure 5A).

While we found that the prior therapy significantly impacted the immune microenvironment composition at baseline, iberdomide remained pharmacodynamically active across all patient subsets. This included increasing the abundance of CD8$^+$ T cells, NK cells, and NKT cells in the tumor microenvironment in patients who have previously received an IMiD, anti-CD38 mAb therapy, or BCMA-targeted therapy. Furthermore, all the major immune cell population changes in triple-class refractory patients (i.e., patients with disease refractory to ≥ 1 immunomodulatory drug, ≥ 1 proteasome inhibitor, and ≥ 1 anti-CD38 mAb) were consistent with those in the cohort overall (Figure S11). In patients who were treated with anti-CD38 mAb immediately prior to study enrollment ($n = 27$), who demonstrated lower relative abundance of NK cells at the screening time point, a significant increase of total NK cells (both CD56$^+$ and CD16$^+$) was seen. Furthermore, an increase in proliferating or activated NK cells expressing markers such as Ki-67, GZMB, and NKG2D was comparable for patients immediately after treatment with anti-CD38 mAb therapy, compared to all others (Figure 5B). In patients who were treated with pomalidomide immediately prior to study enrollment ($n = 26$), the increase in NK, NKT, and EM CD4$^+$/CD8$^+$ T cells was significant and comparable to the other patients (Figure 5C). Additionally, the changes in the abundance of CD8$^+$ T cells and NK cells expressing activation and exhaustion markers were similar for most markers including CD8$^+$Ki-67$^+$, CD8$^+$HLA-DR$^+$, and CD8$^+$TIGIT$^+$ T cells, further supporting the immunostimulatory effect of iberdomide across this heavily pretreated population, including patients refractory to other immunomodulatory drugs.

Changes in T, B, and NK cells were also observed systemically in the peripheral blood

To elucidate whether the observed changes in the TME were the result of trafficking of immune cell populations into the bone marrow, we analyzed changes of relative immune populations in the peripheral blood on the same cohort of patients, as shown in Figure S12. In the peripheral blood from matched patients, flow cytometry data showed a significant relative decrease of B cells ($p < 0.001$), whereas percentages of T and NK cells remained stable and CD14$^+$ monocytes increased significantly ($p < 0.001$). Ki-67$^+$ T and NK cells also increased (median 6.2%

Cell Reports Medicine
Article

CellPress
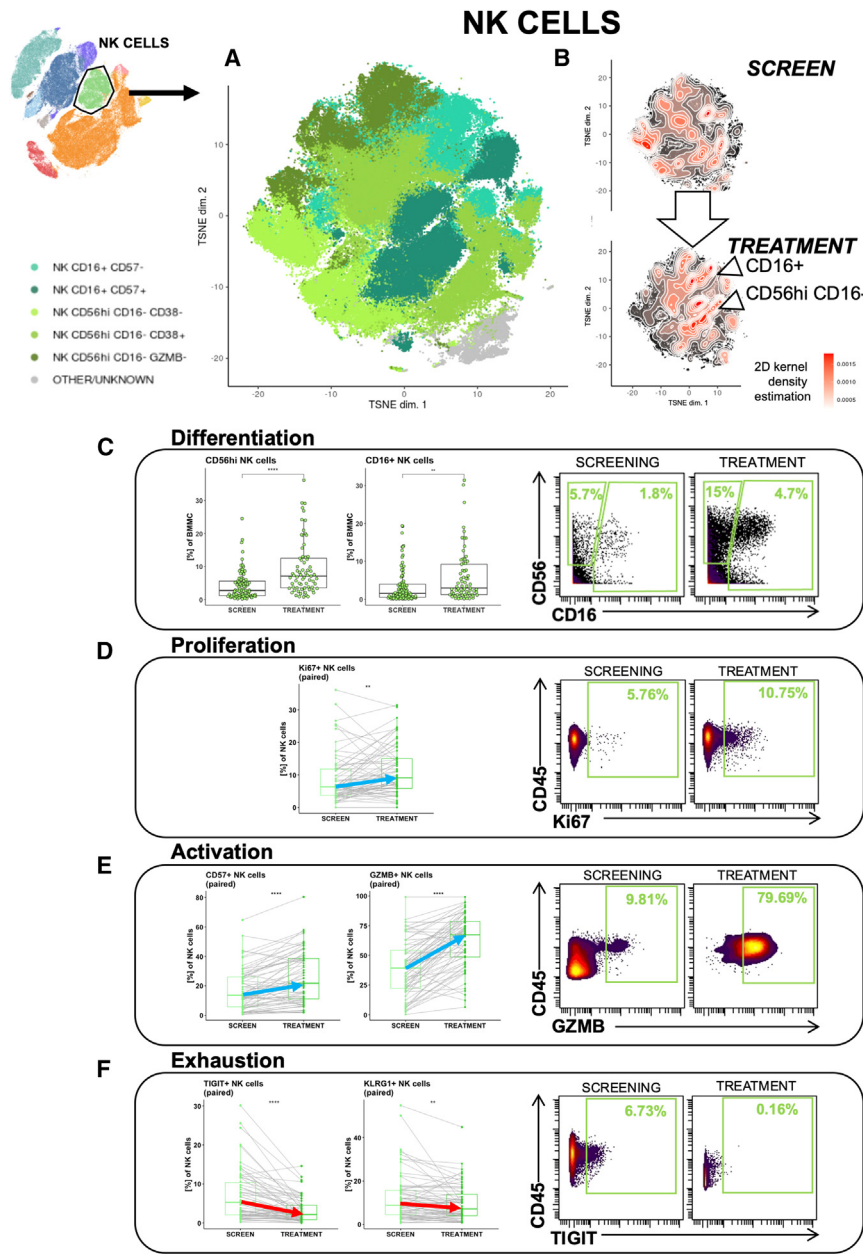OPEN ACCESS

Figure 4. Mid-cycle 2 changes (C2D15) of the NK cell phenotype following iberdomide treatment demonstrate differentiation, proliferation, and activation

(A) t-SNE representation of NK of all (n = 93) patients included in the analysis at both time points. The cells were clustered using a FlowSOM-based clustering strategy, and clusters were manually annotated based on expression of canonical markers. While all cells were included in the clustering analysis, a subset of 1,000 cells were randomly selected for inclusion in the t-SNE plot.

(B) t-SNE plot of NK cells of all (n = 93) patients included in the analysis at both time points, split between cells collected before treatment with iberdomide ± dexamethasone (screen, top) and at the C2D15 time point (treatment, bottom). Individual cells are shown as black dots. A random sample of 1,000 cells per sample was selected for inclusion in the plot. The overlaying heatmap in red corresponds to a 2D kernel density estimation showing the abundance of cell populations on the t-SNE plot, where areas in bright red correspond to a high local abundance of cells.

(C) Relative abundances of CD56^bright NK cells and CD16+ NK cells as a percentage of BMMCs, shown before treatment with iberdomide ± dexamethasone (screen) and at the C2D15 time point (treatment). The shift is illustrated by a representative dot plot showing the percentage of the BMMC gate (right).

(D) Relative abundances of NK cells expressing the proliferation marker Ki-67 as a percentage of all NK cells (parent population) within paired samples, shown before treatment with iberdomide ± dexamethasone (screen) and at the C2D15 time point (treatment). The change between time points is illustrated by a representative dot plot (right) showing the percentage of the parent population gate.

(E) Relative abundances of NK cells expressing the activation markers CD57 and GZMB as a percentage of all NK cells (parent population) within paired samples, shown before treatment with iberdomide ± dexamethasone (screen) and at the C2D15 time point (treatment). The change between time points is illustrated by a representative dot plot (right) showing the percentage of the parent population gate.

(F) Relative abundances of NK cells expressing the exhaustion marker TIGIT and the senescence

marker KLRG1 as a percentage of all NK cells (parent population) within paired samples, shown before treatment with iberdomide ± dexamethasone (screen) and at the C2D15 time point (treatment). The change between time points is illustrated by a representative dot plot (right) showing the percentage of the parent population gate.

In (C)–(F), each dot on the boxplot represents a patient sample. Arrows illustrate the change in the median proportion. Boxplots show median, Q1 and Q3 quartiles, and whiskers up to 1.5× interquartile range (****p < 0.0001, ***p < 0.001, **p < 0.01, *p < 0.05, and ns, $p \geq$ 0.05, Mann-Whitney U test). On the flow cytometry dot-plot, each dot corresponds to a single cell.

See also Figure S9.

vs. 15.6% of T cells, median 14.5% vs. 25.4% of NK cells, both p < 0.001), and within the CD8+ T cells, naive cells decreased (median 5.4% vs. 0.8% of CD8+ T cells), while EM cells expanded (median 37.2% vs. 60.6% of CD8+ T cells). While peripheral blood mononuclear cells were stained with a limited set of markers for flow cytometry and did not exactly match those determined in the bone marrow by mass cytometry, the consistent immune cell subset changes between bone marrow tumor microenvironment (TME) and peripheral blood suggest a systemic effect of iberdomide.

In Figure 6, we synthesize the findings of the various effects of iberdomide in the bone marrow microenvironment in MM.
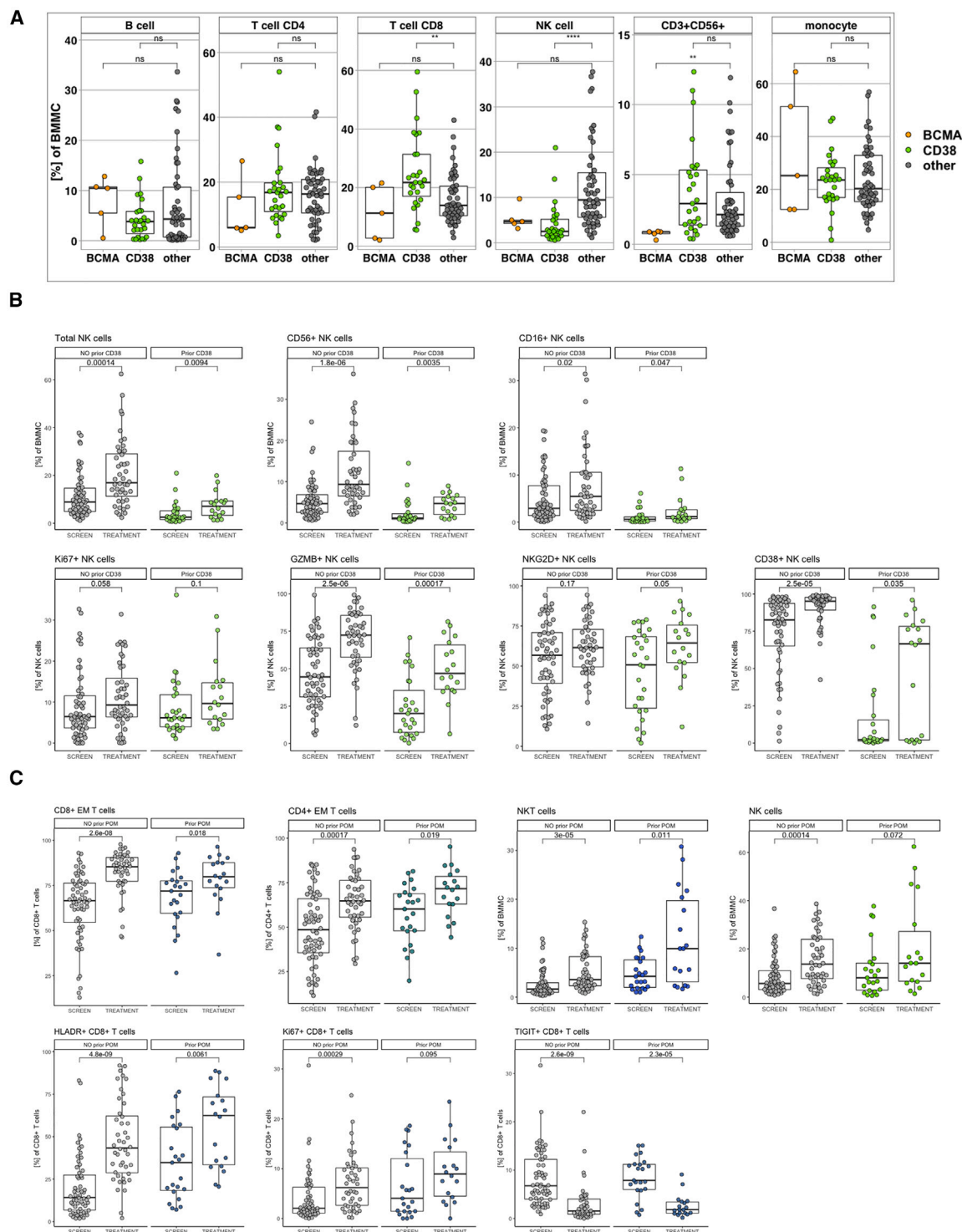
Figure 5. Immediate prior therapy regimen variability is associated with differential composition of the immune microenvironment of patients with relapsed/refractory multiple myeloma, and immune changes are observed despite immediately prior pomalidomide therapy

(A) Relative abundances of major immune cell populations (B cells, $CD4^+$ T cells, $CD8^+$ T cells, NK cells, NKT [$CD3^+$ $CD56^+$] cells, and monocytes) as a percentage of BMMCs, shown before treatment with iberdomide ± dexamethasone (i.e., screening time point) split by last treatment prior to study enrollment, highlighting patients with immediately prior BCMA-targeted treatment (BCMA, orange, $n = 5$) and immediately prior regimens containing anti-CD38 monoclonal antibody (mAb) (CD38, green, $n = 27$) vs. all other treatment regimens (gray).
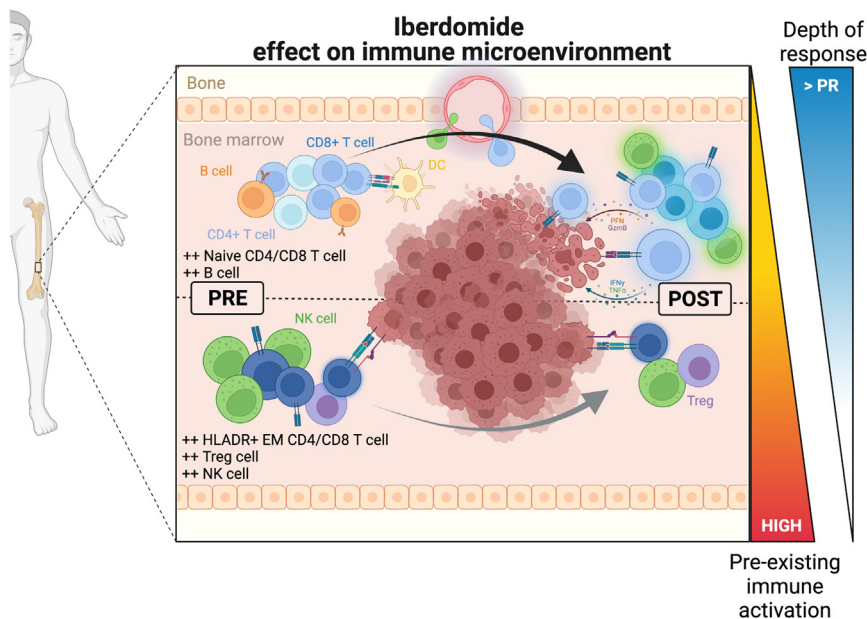
(legend continued on next page)

Cell Reports Medicine
Article

CellPress
OPEN ACCESS

Figure 6. Graphical summary of the proposed immunomodulatory effects of iberdomide on the bone marrow microenvironment of patients with RRMM

Iberdomide caused T and NK cell activation and proliferation in a dose-dependent manner. Higher proportions of naive CD4$^+$/CD8$^+$ cells and B cells were associated with deeper responses, whereas increased Treg cells, activated (HLA-DR$^+$) EM CD4/CD8 T cells, and NK cells were associated with decreased response, overall consistent with a model where immune activation contributes to clinical response in addition to the direct antitumor cytotoxicity of iberdomide.

DISCUSSION

The CELMoD agent iberdomide, in combination with dexamethasone and other agents, has shown promising efficacy for patients with myeloma in early phase trials. In this large multicenter study across two continents, we were able to develop and standardize a reproducible mass cytometry workflow to investigate the impact of iberdomide on the bone marrow microenvironment of patients with RRMM. In doing so, we analyzed longitudinal bone marrow samples from one of the largest cohorts of patients with RRMM at single-cell resolution, with appropriate statistical power, including patients who were refractory to lenalidomide, pomalidomide, anti-CD38 mAb, and BCMA-targeted therapy. Our work not only shows that immune monitoring of the (bone

marrow) TME using a multiplex proteomic assay at single-cell resolution is feasible but that serial sampling for the identification of biomarkers of response to immune-mediated therapies can be applied to future trials or in the clinic.

We described a quantifiable immune phenotype of naive, non-activated T cells at baseline and subsequent immune activation, associated with objective response, whereas patients having pre-existing or persistent T/NK cell proliferation and activation in the bone marrow or high levels of Treg cells were less likely to respond. These findings establish the potential for our workflow to be used for similar biomarker discovery in the context of other immune-mediated treatment strategies that have been approved or are being studied in patients with myeloma, including T cell-engaging therapies. The correlation of specific immune cell abundances with both objective response and iberdomide dose support the hypothesis that the immunomodulatory changes are associated with iberdomide treatment and that stimulation of the immune microenvironment contributes significantly to its mechanism of action, leading to clinical benefit.

We also observed that the last prior therapy had a profound impact on the composition of the tumor immune microenvironment at baseline. This finding suggests that studying the bone marrow microenvironment may have consequences for optimal

(B) Relative abundances of selected immune cell populations (NK cells, CD56$^+$ NK cells, CD16$^+$ NK cells, and NK cells positive for Ki-67, GZMB, NKG2D, and CD38, respectively) as a percentage of the parent population (indicated on the y axis), shown before treatment with iberdomide ± dexamethasone (screen) and at the C2D15 time point (treatment). Samples were split in a group without CD38 mAb exposure immediately prior to study enrollment (no prior CD38, $n = 56$) and a group with immediately prior CD38 mAb exposure (prior CD38, $n = 27$). Each dot represents a patient sample. Boxplots show median, Q1 and Q3 quartiles, and whiskers up to 1.5× interquartile range (****$p < 0.0001$, ***$p < 0.001$, **$p < 0.01$, *$p < 0.05$, and ns, $p \geq 0.05$, Mann-Whitney U test).

(C) Relative abundances of selected immune cell populations (EM [CD45RA$^-$CCR7$^-$] CD8$^+$ T cells, EM CD4$^+$ T cells, NKT cells, NK cells, HLA-DR$^+$CD8$^+$ T cells, Ki-67$^+$CD8$^+$ T cells, and TIGIT$^+$CD8$^+$ T cells) as a percentage of parent population (indicated on the y axis), shown before treatment with iberdomide ± dexamethasone (screen) and at the C2D15 time point (treatment). Samples were split in a group without pomalidomide (POM) exposure immediately prior to study enrollment (no prior POM, $n = 60$) and a group with immediately prior POM exposure (prior POM, $n = 26$). Each dot represents a patient sample. Boxplots show median, Q1 and Q3 quartiles, and whiskers up to 1.5× interquartile range (****$p < 0.0001$, ***$p < 0.001$, **$p < 0.01$, *$p < 0.05$, and ns, $p \geq 0.05$, Mann-Whitney U test).

See also Figures S10 and S11.

sequencing of treatment strategies in MM, particularly given the rising importance of treatment strategies leveraging different aspects of the immune system in the treatment of myeloma. Despite the differences at baseline, phenotypic changes suggesting proliferation, activation, and differentiation of T and NK cells were comparable across RRMM regardless of prior therapeutic journey, including the patients with triple-class refractory disease or the patients treated with pomalidomide-containing regimens immediately prior to the study. Resistance to IMiDs due to genetic events leading to reduced expression or loss of function of the CRBN E3 ligase have been previously reported, including mutations, splice variants and copy loss of CRBN itself, and alterations of the COP9 signalosome.[37–39] Additionally, other genetic and epigenetic changes may indirectly contribute to IMiD resistance. A companion manuscript[40] includes data showing the on-target activity on Ikaros and Aiolos, as well as a genomic analysis of patients in this trial, showing clinical responses across all patient subgroups, including those with CRBN dysregulation, further supporting the importance of an immune-mediated mechanism for iberdomide.

Overall, we found significant phenotypic changes suggesting the differentiation, activation, and proliferation of T and NK cell populations in the bone marrow and peripheral blood of heavily pretreated patients with MM. Both CD4$^+$ and CD8$^+$ T cells shifted from a naive to an EM phenotype. Iberdomide treatment was also associated with a depletion of baseline immunophenotypes suggestive of exhaustion, including T and NK cells expressing TIGIT. The mechanism for this significant reduction in TIGIT expression is unclear. Further research is necessary to study if and how Ikaros and Aiolos degradation in T cells is related to the downregulation of inhibitory checkpoints, as this could offer an alternative strategy to use CELMoD agents to improve the efficacy of T cell-redirecting therapies such as CAR T cells or bispecific antibodies. Additionally, these data provide clinical rationale for iberdomide to enhance the activity of checkpoint inhibitors, including anti-TIGIT therapies.

In summary, this study provides evidence that treatment with iberdomide is associated with significant activation and proliferation of innate and adaptive immune cell populations in the tumor microenvironment of patients with RRMM, without causing exhaustion. These findings support future studies with rational combinations of iberdomide and other agents in myeloma, including T cell-redirecting therapies (i.e., antibodies or cell-based therapies), to further improve therapeutic outcomes with this potent CELMoD agent.

Limitations of the study

Our study aims to characterize how iberdomide treatment changes the immune phenotype of the TME in patients with MM. We show phenotypically that there is significant proliferation, differentiation, and activation of cell populations of the innate and adaptive immune system, suggesting an immune-mediated mechanism of action for the CELMoD agent. While the analyses presented in this work are comprehensive, important limitations remain. Only a small subset of patients was treated with iberdomide monotherapy, whereas most patients were treated with the combination of iberdomide and dexa-

methasone, confounding the effects of both drugs to some extent. In addition to the phenotypic analysis presented here, functional experiments would help demonstrate the extent to which iberdomide improves antitumor cytotoxicity and cytokine production. The data presented here were collected as part of a clinical trial, which leads to intrinsic limitations in terms of sample size, sample availability, and follow-up time. As the data continue to mature, it would be of interest to confirm that the observed immune changes correlate to duration of response. Furthermore, there were not enough samples collected at the time of relapse to study whether the immune changes were reversible. We acknowledge that it remains possible that some of the observed changes in the TME are the result of iberdomide's direct antitumoral effect on myeloma cells resulting in a different bone marrow niche (rather than a direct effect of iberdomide on immune cells). An accompanying manuscript addresses specifically how the various mechanisms of action contribute to the clinical response to iberdomide.[40]

STAR★METHODS

Detailed methods are provided in the online version of this paper and include the following:

- KEY RESOURCES TABLE
- RESOURCE AVAILABILITY
  - Lead contact
  - Materials availability
  - Data and code availability
- EXPERIMENTAL MODEL AND STUDY PARTICIPANT DETAILS
  - Study objectives and design
  - Study population
- METHOD DETAILS
  - Sample collection and tissue processing
  - Mass cytometry
- QUANTIFICATION AND STATISTICAL ANALYSIS
  - Mass cytometry data analysis
  - Statistical considerations
- ADDITIONAL RESOURCES

SUPPLEMENTAL INFORMATION

Supplemental information can be found online at https://doi.org/10.1016/j.xcrm.2024.101584.

AUTHOR CONTRIBUTIONS

M.A., E.F., S.G., M.M., S.J., W.E.P., U.O., A.T., and S.P. provided conceptualization, methodology, analysis, resources, and supervision of the research project. O.V.O., M.A., M.G., B.U., A.P.C., G.K., M.P., S.K.-S., A.L., S.G., W.E.P., U.O., and S.P. were involved in the design, execution, interpretation, and analysis of immunological assays. O.V.O., M.A., M.G., and A.L. conducted computational data analyses including statistical methodology and creation of

Cell Reports Medicine
Article

CellPress

OPEN ACCESS

REFERENCES

1. McCarthy, P.L., Holstein, S.A., Petrucci, M.T., Richardson, P.G., Hulin, C., Tosi, P., Bringhen, S., Musto, P., Anderson, K.C., Caillot, D., et al. (2017). Lenalidomide Maintenance After Autologous Stem-Cell Transplantation in Newly Diagnosed Multiple Myeloma: A Meta-Analysis. J. Clin. Oncol. 35, 3279–3289. https://doi.org/10.1200/jco.2017.72.6679.

2. Richardson, P.G., Siegel, D.S., Vij, R., Hofmeister, C.C., Baz, R., Jagannath, S., Chen, C., Lonial, S., Jakubowiak, A., Bahlis, N., et al. (2014). Pomalidomide alone or in combination with low-dose dexamethasone in relapsed and refractory multiple myeloma: a randomized phase 2 study. Blood 123, 1826–1832. https://doi.org/10.1182/blood-2013-11-538835.

3. Benboubker, L., Dimopoulos, M.A., Dispenzieri, A., Catalano, J., Belch, A.R., Cavo, M., Pinto, A., Weisel, K., Ludwig, H., Bahlis, N., et al. (2014). Lenalidomide and Dexamethasone in Transplant-Ineligible Patients with Myeloma. N. Engl. J. Med. 371, 906–917. https://doi.org/10.1056/NEJMoa1402551.

4. Miguel, J.S., Weisel, K., Moreau, P., Lacy, M., Song, K., Delforge, M., Karlin, L., Goldschmidt, H., Banos, A., Oriol, A., et al. (2013). Pomalidomide plus low-dose dexamethasone versus high-dose dexamethasone alone for patients with relapsed and refractory multiple myeloma (MM-003): a randomised, open-label, phase 3 trial. Lancet Oncol. 14, 1055–1066. https://doi.org/10.1016/S1470-2045(13)70380-2.

5. Rajkumar, S.V., Jacobus, S., Callander, N.S., Fonseca, R., Vesole, D.H., Williams, M.E., Abonour, R., Siegel, D.S., Katz, M., and Greipp, P.R.; Eastern Cooperative Oncology Group (2010). Lenalidomide plus high-dose dexamethasone versus lenalidomide plus low-dose dexamethasone as initial therapy for newly diagnosed multiple myeloma: an open-label randomised controlled trial. Lancet Oncol. 11, 29–37. https://doi.org/10.1016/S1470-2045(09)70284-0.

6. Ito, T., Ando, H., Suzuki, T., Ogura, T., Hotta, K., Imamura, Y., Yamaguchi, Y., and Handa, H. (2010). Identification of a primary target of thalidomide teratogenicity. Science 327, 1345–1350. https://doi.org/10.1126/science.1177319.

7. Lopez-Girona, A., Mendy, D., Ito, T., Miller, K., Gandhi, A.K., Kang, J., Karasawa, S., Carmel, G., Jackson, P., Abbasian, M., et al. (2012). Cereblon is a direct protein target for immunomodulatory and antiproliferative activities of lenalidomide and pomalidomide. Leukemia 26, 2326–2335. https://doi.org/10.1038/leu.2012.119.

8. Alzoman, N.Z., Darwish, I.A., and Abuhejail, R.M. (2014). A highly sensitive polyclonal antibody-based ELISA for therapeutic monitoring and pharmacokinetic studies of lenalidomide. J. Immunoassay Immunochem. 35, 130–138. https://doi.org/10.1080/15321819.2013.824898.

9. Bjorklund, C.C., Lu, L., Kang, J., Hagner, P.R., Havens, C.G., Amatangelo, M., Wang, M., Ren, Y., Couto, S., Breider, M., et al. (2015). Rate of CRL4CRBN substrate Ikaros and Aiolos degradation underlies differential activity of lenalidomide and pomalidomide in multiple myeloma cells by regulation of c-Myc and IRF4. Blood Cancer J. 5, e354. https://doi.org/10.1038/bcj.2015.66.

10. John, L.B., and Ward, A.C. (2011). The Ikaros gene family: transcriptional regulators of hematopoiesis and immunity. Mol. Immunol. 48, 1272–1278. https://doi.org/10.1016/j.molimm.2011.03.006.

11. Gandhi, A.K., Kang, J., Capone, L., Parton, A., Wu, L., Zhang, L.H., Mendy, D., Lopez-Girona, A., Tran, T., Sapinoso, L., et al. (2010). Dexamethasone synergizes with lenalidomide to inhibit multiple myeloma tumor growth, but reduces lenalidomide-induced immunomodulation of T and NK cell function. Curr. Cancer Drug Targets 10, 155–167.

12. Kronke, J., Udeshi, N.D., Narla, A., Grauman, P., Hurst, S.N., McConkey, M., Svinkina, T., Heckl, D., Comer, E., Li, X., et al. (2014). Lenalidomide causes selective degradation of IKZF1 and IKZF3 in multiple myeloma cells. Science 343, 301–305. https://doi.org/10.1126/science.1244851.

13. Li, S., Pal, R., Monaghan, S.A., Schafer, P., Ouyang, H., Mapara, M., Galson, D.L., and Lentzsch, S. (2011). IMiD immunomodulatory compounds block C/EBPβ translation through eIF4E down-regulation resulting in inhibition of MM. Blood 117, 5157–5165. https://doi.org/10.1182/blood-2010-10-314278.

14. Ma, S., Pathak, S., Mandal, M., Trinh, L., Clark, M.R., and Lu, R. (2010). Ikaros and Aiolos inhibit pre-B-cell proliferation by directly suppressing c-Myc expression. Mol. Cell Biol. 30, 4149–4158. https://doi.org/10.1128/MCB.00224-10.

15. Schmitt, C., Tonnelle, C., Dalloul, A., Chabannon, C., Debré, P., and Rebollo, A. (2002). Aiolos and Ikaros: regulators of lymphocyte development, homeostasis and lymphoproliferation. Apoptosis 7, 277–284. https://doi.org/10.1023/a:1015372322419.

16. Zhu, Y.X., Braggio, E., Shi, C.X., Bruins, L.A., Schmidt, J.E., Van Wier, S., Chang, X.B., Bjorklund, C.C., Fonseca, R., Bergsagel, P.L., et al. (2011). Cereblon expression is required for the antimyeloma activity of lenalidomide and pomalidomide. Blood 118, 4771–4779. https://doi.org/10.1182/blood-2011-05-356063.

17. Gandhi, A.K., Kang, J., Havens, C.G., Conklin, T., Ning, Y., Wu, L., Ito, T., Ando, H., Waldman, M.F., Thakurta, A., et al. (2014). Immunomodulatory agents lenalidomide and pomalidomide co-stimulate T cells by inducing degradation of T cell repressors Ikaros and Aiolos via modulation of the E3 ubiquitin ligase complex CRL4(CRBN). Br. J. Haematol. 164, 811–821. https://doi.org/10.1111/bjh.12708.

18. Hagner, P.R., Chiu, H., Ortiz, M., Apollonio, B., Wang, M., Couto, S., Waldman, M.F., Flynt, E., Ramsay, A.G., Trotter, M., et al. (2017). Activity of lenalidomide in mantle cell lymphoma can be explained by NK cell-mediated cytotoxicity. Br. J. Haematol. 179, 399–409. https://doi.org/10.1111/bjh.14866.

19. LeBlanc, R., Hideshima, T., Catley, L.P., Shringarpure, R., Burger, R., Mitsiades, N., Mitsiades, C., Cheema, P., Chauhan, D., Richardson, P.G., et al. (2004). Immunomodulatory drug costimulates T cells via the B7-CD28 pathway. Blood 103, 1787–1790. https://doi.org/10.1182/blood-2003-02-0361.

20. Neuber, B., Dai, J., Waraich, W.A., Awwad, M.H.S., Engelhardt, M., Schmitt, M., Medenhoff, S., Witzens-Harig, M., Ho, A.D., Goldschmidt, H., and Hundemer, M. (2017). Lenalidomide overcomes the immunosuppression of regulatory CD8+ CD28− T-cells. Oncotarget 8, 98200–98214.

21. Schafer, P.H., Gandhi, A.K., Loveland, M.A., Chen, R.S., Man, H.-W., Schnetkamp, P.P.M., Wolbring, G., Govinda, S., Corral, L.G., Payvandi, F., et al. (2003). Enhancement of cytokine production and AP-1 transcriptional activity in T cells by thalidomide-related immunomodulatory drugs. J. Pharmacol. Exp. Ther. 305, 1222–1232.

22. Noonan, K., Rudraraju, L., Ferguson, A., Emerling, A., Pasetti, M.F., Huff, C.A., and Borrello, I. (2012). Lenalidomide-induced immunomodulation in

multiple myeloma: impact on vaccines and antitumor responses. Clin. Cancer Res. *18*, 1426–1434.

23. Lioznov, M., El-Cheikh, J., Hoffmann, F., Hildebrandt, Y., Ayuk, F., Wolschke, C., Atanackovic, D., Schilling, G., Badbaran, A., Bacher, U., et al. (2010). Lenalidomide as salvage therapy after allo-SCT for multiple myeloma is effective and leads to an increase of activated NK (NKp44+) and T (HLA-DR+) cells. Bone Marrow Transplant. *45*, 349–353.

24. Rychak, E., Mendy, D., Shi, T., Ning, Y., Leisten, J., Lu, L., Miller, K., Narla, R.K., Orlowski, R.Z., Raymon, H.K., et al. (2016). Pomalidomide in combination with dexamethasone results in synergistic anti-tumour responses in pre-clinical models of lenalidomide-resistant multiple myeloma. Br. J. Haematol. *172*, 889–901.

25. Sehgal, K., Das, R., Zhang, L., Verma, R., Deng, Y., Kocoglu, M., Vasquez, J., Koduru, S., Ren, Y., Wang, M., et al. (2015). Clinical and pharmacodynamic analysis of pomalidomide dosing strategies in myeloma: impact of immune activation and cereblon targets. Blood *125*, 4042–4051. https://doi.org/10.1182/blood-2014-11-611426.

26. Croft, J., Hall, A., Walker, K., Sherborne, A.L., Boyd, K., Garg, M., Pawlyn, C., Sherratt, D., Reed, S., Pierceall, W.E., et al. (2018). Cyclophosphamide exerts significant immunomodulatory function in myeloma patients treated with pomalidomide and dexamethasone. Blood *132*, 4482.

27. Pierceall, W.E., Amatangelo, M.D., Bahlis, N.J., Siegel, D.S., Rahman, A., Van Oekelen, O., Neri, P., Young, M., Chung, W., Serbina, N., et al. (2020). Immunomodulation in Pomalidomide, Dexamethasone, and Daratumumab-Treated Patients with Relapsed/Refractory Multiple Myeloma. Clin. Cancer Res. *26*, 5895–5902. https://doi.org/10.1158/1078-0432.Ccr-20-1781.

28. Van Oekelen, O., Parekh, S., Cho, H.J., Vishnuvardhan, N., Madduri, D., Richter, J., Ip, C., Lau, K., Florendo, E., Mancia, I.S., et al. (2020). A phase II study of pomalidomide, daily oral cyclophosphamide, and dexamethasone in relapsed/refractory multiple myeloma. Leuk. Lymphoma *61*, 2208–2215. https://doi.org/10.1080/10428194.2020.1805111.

29. Matyskiela, M.E., Zhang, W., Man, H.W., Muller, G., Khambatta, G., Baculi, F., Hickman, M., LeBrun, L., Pagarigan, B., Carmel, G., et al. (2018). A Cereblon Modulator (CC-220) with Improved Degradation of Ikaros and Aiolos. J. Med. Chem. *61*, 535–542. https://doi.org/10.1021/acs.jmedchem.6b01921.

30. Watson, E.R., Novick, S., Matyskiela, M.E., Chamberlain, P.P., H. de la Peña, A., Zhu, J., Tran, E., Griffin, P.R., Wertz, I.E., and Lander, G.C. (2022). Molecular glue CELMoD compounds are regulators of cereblon conformation. Science *378*, 549–553. https://doi.org/10.1126/science.add7574.

31. Amatangelo, M., Bjorklund, C.C., Kang, J., Polonskaia, A., Viswanatha, S., and Thakurta, A. (2018). Iberdomide (CC-220) Has Synergistic Anti-Tumor and Immunostimulatory Activity Against Multiple Myeloma in Combination with Both Bortezomib and Dexamethasone, or in Combination with Daratumumab in Vitro. Blood *132*, 1935. https://doi.org/10.1182/blood-2018-99-113383.

32. Bjorklund, C.C., Kang, J., Lu, L., Amatangelo, M., Chiu, H., Gandhi, A.K., Pourdehnad, M., Klippel, A., and Thakurta, A. (2016). CC-220 Is a Potent Cereblon Modulating Agent That Displays Anti-Proliferative and Pro-Apoptotic and Immunomodulatory Activity on Sensitive and Resistant Multiple Myeloma Cell Lines. Blood *128*, 1591. https://doi.org/10.1182/blood.V128.22.1591.1591.

33. Amatangelo, M., Van Oekelen, O., Rahman, A.H., Lagana, A., Gooding, S., Avet-Loiseau, H., Oppermann, U., Pierceall, W.E., Thakurta, A., and Parekh, S. (2019). Multidimensional Single Cell Analysis Shows Increased T/NK Cell Subsets in Both Blood and Bone Marrow of Iberdomide (CC-220) Treated Relapsed/Refractory Multiple Myeloma Patients. Blood *134*, 1775. https://doi.org/10.1182/blood-2019-126146.

34. van de Donk, N.W., Popat, R., Larsen, J., Minnema, M.C., Jagannath, S., Oriol, A., Zonder, J., Richardson, P.G., Rodriguez-Otero, P., Badros, A.Z., et al. (2020). First Results of Iberdomide (IBER; CC-220) in Combination with Dexamethasone (DEX) and Daratumumab (DARA) or Bortezomib (BORT) in Patients with Relapsed/Refractory Multiple Myeloma (RRMM). Blood *136*, 16–17. https://doi.org/10.1182/blood-2020-137743.

35. Soni, N., Baturevych, A., Works, M., Qin, J., Balakrishnan, A., and Ports, M. (2020). Iberdomide Increases the Potency of the Anti-BCMA CAR T Cell Product Orvacabtagene Autoleucel (Orva-Cel). In American Society of Gene and Cell Therapy Annual Meeting 2020. https://www.asgct.org/global/documents/asgct20_abstracts_may8?_zs=S2i4b&_zl=U9052.

36. Lonial, S., Popat, R., Hulin, C., Jagannath, S., Oriol, A., Richardson, P.G., Facon, T., Weisel, K., Larsen, J.T., Minnema, M.C., et al. (2022). Iberdomide plus dexamethasone in heavily pretreated late-line relapsed or refractory multiple myeloma (CC-220-MM-001): a multicentre, multicohort, open-label, phase 1/2 trial. Lancet. Haematol. *9*, e822–e832. https://doi.org/10.1016/S2352-3026(22)00290-3.

37. Gooding, S., Ansari-Pour, N., Kazeroun, M., Karagoz, K., Polonskaia, A., Salazar, M., Fitzsimons, E., Sirinukunwattana, K., Chavda, S., Ortiz Estevez, M., et al. (2022). Loss of COP9 signalosome genes at 2q37 is associated with IMiD resistance in multiple myeloma. Blood *140*, 1816–1821. https://doi.org/10.1182/blood.2022015909.

38. Gooding, S., Ansari-Pour, N., Towfic, F., Ortiz Estévez, M., Chamberlain, P.P., Tsai, K.T., Flynt, E., Hirst, M., Rozelle, D., Dhiman, P., et al. (2021). Multiple Cereblon genetic changes associate with acquired resistance to Lenalidomide or Pomalidomide in Multiple Myeloma. Blood *137*, 232–237. https://doi.org/10.1182/blood.2020007081.

39. Kortum, K.M., Mai, E.K., Hanafiah, N.H., Shi, C.X., Zhu, Y.X., Bruins, L., Barrio, S., Jedlowski, P., Merz, M., Xu, J., et al. (2016). Targeted sequencing of refractory myeloma reveals a high incidence of mutations in CRBN and Ras pathway genes. Blood *128*, 1226–1233. https://doi.org/10.1182/blood-2016-02-698092.

40. Amatangelo, M., Flynt, E., Stong, N., Ray, P., Van Oekelen, O., Wang, M., Ortiz Estevez, M., Maciag, P.C., Peluso, T., Parekh, S., et al. (2024). Pharmacodynamic changes in tumor and immune cells drive Iberdomide's clinical mechanisms of activity in relapsed and refractory Multiple Myeloma. Cell Reports Medicine *5*, 101571. https://doi.org/10.1016/j.xcrm.2024.101571.

41. Crowell, H.L., Zanotelli, V.R.T., Chevrier, S., and Robinson, M.D. (2020). CATALYST: Cytometry dATa anALYSis Tools.

42. Weber, L.M. (2019). Diffcyt: Differential Discovery in High-Dimensional Cytometry via High-Resolution Clustering.

43. Kumar, S., Paiva, B., Anderson, K.C., Durie, B., Landgren, O., Moreau, P., Munshi, N., Lonial, S., Bladé, J., Mateos, M.V., et al. (2016). International Myeloma Working Group consensus criteria for response and minimal residual disease assessment in multiple myeloma. Lancet Oncol. *17*, e328–e346. https://doi.org/10.1016/s1470-2045(16)30206-6.

44. Zunder, E.R., Finck, R., Behbehani, G.K., Amir, E.A.D., Krishnaswamy, S., Gonzalez, V.D., Lorang, C.G., Bjornson, Z., Spitzer, M.H., Bodenmiller, B., et al. (2015). Palladium-based mass tag cell barcoding with a doublet-filtering scheme and single-cell deconvolution algorithm. Nat. Protoc. *10*, 316–333. https://doi.org/10.1038/nprot.2015.020.

45. Kotecha, N., Krutzik, P.O., and Irish, J.M. (2010). Web-based analysis and publication of flow cytometry experiments. Current protocols in cytometry *Chapter 10*, Unit10.17. https://doi.org/10.1002/0471142956.cy1017s53.

46. Hartmann, F.J., Babdor, J., Gherardini, P.F., Amir, E.A.D., Jones, K., Sahaf, B., Marquez, D.M., Krutzik, P., O'Donnell, E., Sigal, N., et al. (2019). Comprehensive Immune Monitoring of Clinical Trials to Advance Human

Cell Reports Medicine
Article

Immunotherapy. Cell Rep. 28, 819–831.e4. https://doi.org/10.1016/j.celrep.2019.06.049.

47. Nowicka, M., Krieg, C., Crowell, H.L., Weber, L.M., Hartmann, F.J., Guglietta, S., Becher, B., Levesque, M.P., and Robinson, M.D. (2017). CyTOF workflow: differential discovery in high-throughput high-dimensional cytometry datasets. F1000Res. 6, 748. https://doi.org/10.12688/f1000research.11622.2.

48. Ellis, B., Haaland, P., Hahne, F., Le Meur, N., Gopalakrishnan, N., Spidlen, J., Jiang, M., and Finak, G. (2019). flowCore: flowCore: Basic Structures for Flow Cytometry Data.

49. Van Gassen, S., Callebaut, B., Van Helden, M.J., Lambrecht, B.N., Demeester, P., Dhaene, T., and Saeys, Y. (2015). FlowSOM: Using self-organizing maps for visualization and interpretation of cytometry data. Cytometry A. 87, 636–645. https://doi.org/10.1002/cyto.a.22625.

∂ CellPress
OPEN ACCESS

Cell Reports Medicine
Article

STAR★METHODS

KEY RESOURCES TABLE

REAGENT or RESOURCE	SOURCE	IDENTIFIER
Antibodies		
Anti-human CD45 - 89Y	Fluidigm	HI30
Anti-human CD57 - 113In	Biolegend	HNK-1
Anti-human CD11c - 115In	Biolegend	BU15
Anti-human Ki-67 - 141Pr	BD Biosciences	B56
Anti-human CD19 - 142Nd	Miltenyi	REA675
Anti-human CD45RA - 143Nd	Miltenyi	REA562
Anti-human KLRG1 - 144Nd	Biolegend	SA231A2
Anti-human CD4 - 145Nd	Miltenyi	REA623
Anti-human CD8 - 146Nd	Miltenyi	REA734
Anti-human ICOS - 147Sm	Biolegend	C398.4A
Anti-human CD16 - 148Nd	Miltenyi	REA423
Anti-human CD127 - 149Sm	Fluidigm	A019D5
Anti-human CD1c - 150Nd	Miltenyi	REA694
Anti-human CD123 - 151Eu	Miltenyi	REA918
Anti-human CD66b - 152Sm	Miltenyi	REA306
Anti-human TIGIT - 153Eu	Fluidigm	MBSA43
Anti-human TIM3 - 154Sm	Fluidigm	F38-2E2
Anti-human CD27 - 155Gd	Miltenyi	REA499
Anti-human PD-L1 - 156Gd	Biolegend	29E.2A3
Anti-human CD33 - 158Gd	Fluidigm	WM53
Anti-human CD138 - 159Tb	Biolegend	MI15
Anti-human CD14 - 160Gd	Miltenyi	REA599
Anti-human CD56 - 161Dy	Miltenyi	REA196
Anti-human NKG2A - 162Dy	Miltenyi	REA110
Anti-human CD5 - 163Dy	Biolegend	UCHT2
Anti-human CD43 - 164Dy	Biolegend	CD43-10G7
Anti-human NKG2D - 165Ho	Biolegend	1D11
Anti-human CD25 - 166Er	Miltenyi	REA570
Anti-human CCR7 - 167Er	Fluidigm	G043H7
Anti-human CD3 - 168Er	Miltenyi	REA613
Anti-human Tbet - 169Tm	Biolegend	4B10
Anti-human CD38 - 170Er	Miltenyi	REA671
Anti-human CXCR3 - 171Yb	Miltenyi	REA232
Anti-human CD28 - 172Yb	Biolegend	CD28.2
Anti-human CD226 - 173Yb	Biolegend	11A8
Anti-human HLA-DR - 174Yb	Miltenyi	REA805
Anti-human PD-1 - 175Lu	Fluidigm	EH12.2H7
Anti-human GranzymeB - 176Yb	Miltenyi	REA226
Anti-human CD11b - 209Bi	Fluidigm	ICRF44
Biological samples		
Bone marrow aspirates (BMA) from myeloma patients	Multiple clinical study sites	NCT02773030
Peripheral blood from myeloma patients	Multiple clinical study sites	NCT02773030

(Continued on next page)

Cell Reports Medicine
Article

Continued

REAGENT or RESOURCE	SOURCE	IDENTIFIER
Software and algorithms		
Cytobank	Beckman Coulter, Inc.	https://premium.cytobank.org/cytobank/login
R (v3.6.1)	The R Project for Statistical Computing	https://www.r-project.org/
CATALYST	Crowell et al.[41]	https://bioconductor.org/packages/release/bioc/html/CATALYST.html
Diffcyt	Weber et al.[42]	https://bioconductor.org/packages/release/bioc/html/diffcyt.html

RESOURCE AVAILABILITY

Lead contact
- Further information and requests for any additional resources and reagents should be directed to and will be addressed by the lead contact, Dr. Samir Parekh (samir.parekh@mssm.edu).

Materials availability
- The antibodies used for the mass cytometry experiments are detailed in the Key resources table. The concentration used if further specified in Table S1.

Data and code availability
- The cytometry datasets used in this study are from an ongoing clinical trial of iberdomide in multiple myeloma that is sponsored by Bristol Myers Squibb (BMS). The data from this study are stored in Cytobank, an internal database at the Icahn School of Medicine at Mount Sinai, in perpetuity and are not publicly available due to patient privacy concerns and because the clinical trial is still ongoing. To request access to the data, please contact the lead contact (samir.parekh@mssm.edu), and submit a request for access to ctt.group@bms.com. This is the mailbox for BMS' Clinical Trial Transparency (CTT) organization that manages the external distribution of data generated as part of a BMS study. Upon receiving a request, the CTT reviews the request and if approved, will release the data in a properly annotated and de-identified format. The lead contact will help facilitate these requests and will connect you with a member of the CTT organization. Additional questions on submitting a request can be directed to the lead contact or to ctt.group@bms.com at any time and will be promptly addressed. The requestor will be required to describe the objectives of the research project for which the data will be used. Data access will be considered for research purposes and non-commercial use only. To ensure patient privacy, access to personally identifiable information or sensitive clinical information will not be provided, and requests for data access must rigorously adhere to the consent agreements established with study participants.
- This paper does not report original code.
- Any additional information required to reanalyze the data reported in this paper is available from the lead contact upon request.

EXPERIMENTAL MODEL AND STUDY PARTICIPANT DETAILS

Study objectives and design
All samples were obtained from patients enrolled on the CC-220-MM-001 (NCT02773030) phase ½, multicenter, open-label study. This study included dose escalation cohorts of iberdomide as monotherapy (Cohort A) and in combination with dexamethasone (Cohort B) and dose expansion of iberdomide at the recommended phase 2 dose in combination with dexamethasone (Cohort D and Cohort I). Iberdomide was administered on 21 days of a 28-day cycle at doses ranging from 0.3 to 1.0 mg as monotherapy and 0.3 and 1.6 mg in combination with dexamethasone during dose escalation and at 1.6 mg for dose expansion. The starting dose of dexamethasone was 40 mg for subjects who are ≤75 years and 20 mg for subjects who are >75 years, given once weekly. Key eligibility criteria for Cohorts A and B were patients with ≥2 prior lines of therapy, including lenalidomide or pomalidomide and a proteasome inhibitor. Eligibility for Cohort D included patients with ≥3 prior lines of therapy and refractory to both lenalidomide and pomalidomide, as well as proteasome inhibitors, anti-CD38 monoclonal antibodies, and corticosteroids and for Cohort I included ≥3 prior lines of therapy and refractory to lenalidomide, pomalidomide, proteasome inhibitors, anti-CD38 monoclonal antibodies, corticosteroids and a prior BCMA-targeted therapy. Refractory was defined as failure to achieve response or development of progressive disease while on therapy, or progressive disease within 60 days of last dose. The study was conducted in accordance with the International Council for Harmonization Good Clinical Practice Guideline and the general principles outlined in the Declaration of Helsinki. The protocol was approved by each participating center's institutional review board/ethics committee before initiation, and all patients provided written informed consent. In total, 93 eligible subjects enrolled on the CC220-MM-001 study were analyzed, including *n* = 6 patients receiving iberdomide monotherapy (Cohort A) and *n* = 87 patients receiving iberdomide in combination

with dexamethasone (Cohorts B/D/I). A detailed clinical description of the clinical trial, including efficacy and outcome data, have been reported separately.[36]

Study population

The 93 subjects included in this analysis received a median of 5 prior lines of therapy. Most patients in the study cohort were refractory to lenalidomide ($n = 93$, 100%), pomalidomide ($n = 79$, 85%), proteasome inhibitors ($n = 82$, 88%) or CD38 monoclonal antibody therapy ($n = 87$, 94%) and the large majority of patients was triple-class refractory, defined as refractory to ≥ 1 immunomodulatory drug, ≥ 1 proteasome inhibitor, and ≥ 1 CD38 monoclonal antibody ($n = 77$, 83%). Overall, 30 of 93 subjects treated achieved an objective response (i.e., partial response (PR) or better according to International Myeloma Working Group (IMWG) criteria[43]) for an objective response rate (ORR) of 32%. Across the cohort, 8 subjects achieved a very good partial response (VGPR). Notably, patient demographics and responses for the biomarker subpopulation were comparable to the intent-to-treat population. A summary of the demographics and responses is shown in see below table.

Clinical and disease characteristics of the study cohort

	CC220-MM-001 CyTOF	CC220-MM-001 (cohorts A, B, and C)
Total patients, *n*	93	197
Median age (range), years	66 (44–82)	65 (33–83)
Patients aged ≥ 75 years, *n* (%)	13 (13.98)	31 (15.74)
Male, *n* (%)	45 (48.39)	103 (52.28)
ECOG (Eastern Cooperative Oncology Group) performance status		
0	31 (33.33)	73 (37.06)
1	58 (62.37)	105 (53.3)
2	4 (4.3)	19 (9.64)
Cytogenetic risk category, *n* (%)		
High[a]	24 (25.81)	46 (23.35)
Standard[b]	14 (15.05)	29 (14.72)
Missing	55 (59.14)	122 (61.93)
Median time since diagnosis (range), years	7.4 (2.2–24.8)	7.2 (1.6–24.5)
ISS (International Staging System) stage at study entry, *n* (%)		
I	51 (54.84)	89 (45.18)
II	27 (29.03)	71 (36.04)
III	15 (16.13)	37 (18.78)
Prior stem cell transplant, *n* (%)	77 (82.8)	158 (80.2)
Number of prior therapies median (range)	5 (2–17)	5 (2–23)
Type of prior treatment, *n* (%)		
Immunomodulatory drugs and proteasome inhibitors	82 (88.17)	172 (87.31)
Lenalidomide	93 (100)	197 (100)
Pomalidomide	82 (88.17)	170 (86.29)
Bortezomib	93 (100)	195 (98.98)
Carfilzomib	58 (62.37)	117 (59.39)
Daratumumab	84 (90.32)	167 (84.77)
Isatuximab	3 (3.23)	10 (5.08)
BCMA-targeted therapy	7 (7.53)	0 (0.00)
Refractory to prior treatment, *n* (%)		
Immunomodulatory drugs	92 (98.92)	193 (97.97)
Lenalidomide	93 (100)	197 (100)
Pomalidomide	79 (84.95)	159 (80.71)
Proteasome inhibitors	82 (88.17)	174 (88.32)
CD38 monoclonal antibodies	87 (93.55)	174 (88.32)
Triple-class refractory[c]	77 (82.8)	157 (79.7)

(Continued on next page)

Cell Reports Medicine
Article

CellPress
OPEN ACCESS

Continued

	CC220-MM-001 CyTOF	CC220-MM-001 (cohorts A, B, and C)
Extramedullary plasmacytomas, *n* (%)		
Yes	17 (18.28)	43 (21.83)
No	76 (81.72)	154 (78.17)
Pomalidomide in last line of treatment	26 (27.96)	49 (24.87)

[a]Defined as the presence of any abnormality for del(17p), and/or translocation t(4:14), and/or translocation t(14,16), and/or amplification 1q21.
[b]Defined as the absence of abnormality for del(17p), translocation t(4:14), translocation t(14,16), and amplification 1q21.
[c]Defined as refractory to ≥1 immunomodulatory drug, ≥1 proteasome inhibitor, and ≥1 anti-CD38 monoclonal antibody.

METHOD DETAILS

Sample collection and tissue processing

All patients provided consent for correlative studies. Baseline evaluation included collection of peripheral blood and bone marrow aspirate. Patients had post-treatment peripheral blood samples collected pre-dose cycle (C) 1 day (D) 1, C2D15 and end of treatment. Bone marrow aspirates were collected pre-dose during screening period, post-dose at C2D15 and requested at the end of treatment visit (Figure 1). Bone marrow aspirates of subjects treated in either the United States or Europe were sent overnight directly to the Icahn School of Medicine at Mount Sinai, New York (United States) or Oxford University (United Kingdom) respectively. Bone marrow mononuclear cells (BMMC) or peripheral blood mononuclear cells (PBMC) were isolated by Ficoll separation. Cells were counted and stored in FBS/10% DMSO in liquid nitrogen until analysis. For all 93 subjects, at least one sample was analyzed and for 66 subjects, both the baseline and the on-treatment sample were available.

Mass cytometry

Cells were stained with the mass cytometry (CyTOF) antibody panel listed in Table S1. All antibodies were either purchased pre-conjugated from Fluidigm or conjugated at the Human Immune Monitoring Center, Icahn School of Medicine at Mount Sinai, using commercial X8 polymer conjugation kits purchased from Fluidigm. All conjugated antibodies were tittered and validated on healthy donor PBMCs. For longitudinal monitoring of phenotypic changes, cells from selected timepoints were thawed, counted, and assessed for viability utilizing the Nexcelom Cellaca Automated Cell Counter (Nexcelom Bioscience, Lawrence, MA, USA) along with acridine orange/propidium iodine staining (Nexcelom Bioscience, Lawrence, MA, USA). For sample timepoint batching, live-cell CyTOF barcoding was performed using anti-B2M antibodies conjugated to cadmium isotopes (Cd 111, 112, 114, and 116). Rhodium-103 viability and Human TruStain FcX staining (BioLegend) was performed simultaneously at room temperature for 30 min. After cell washing in flow cytometry buffer (1x PBS + 0.2% BSA + 0.05% NaN3), patient timepoints were combined and cells were stained with a cocktail of surface antibodies (Table S2). Surface-stained cells were then fixed with 1.6% formaldehyde. In a second step, each patient was barcoded with the CyTOF Cell-ID 20-Plex Palladium Barcoding Kit (Fluidigm) (using Pd 102, 104, 105, 106, 108, and 110 isotopes). Barcoded cells were fixed and permeabilized with Fix-Perm buffer (BD Biosciences) and stained with the remaining intracellular antibodies from the panel. Stained samples were finally fixed in freshly diluted 4% paraformaldehyde containing 125nM intercalator-Ir (Fluidgm) and 300nM OsO4 (ACROS Organics) and stored at −80°C in FBS+10%DMSO. Samples for mass cytometry acquisition were washed with cell staining buffer (Fluidigm) and re-suspended in CAS buffer containing EQ normalization beads (Fluidigm) and acquired on a CyTOF2 instrument (Fluidigm). Post-acquisition, the data was normalized using bead-based normalization algorithm in the CyTOF software (Fluidigm). Normalized data was de-barcoded using methods and software developed at the Stanford University School of Medicine.[44] Normalized and de-barcoded data was uploaded to Cytobank[45] for final analysis as detailed below.

QUANTIFICATION AND STATISTICAL ANALYSIS

Mass cytometry data analysis

Data was visualized and manual gating was performed using Cytobank.[45] A set of prespecified populations was hierarchically gated using the workflow by Hartmann et al.[46] as a scaffold (Figures 1 and S2) and summary statistics (i.e., relative population frequencies) were exported from Cytobank. To minimize bias, hierarchical gating of the American and European cohorts was conducted by two different investigators independently and data were analyzed separately, in which the European cohort was used as a validation set. As findings were generally consistent across both cohorts (Figure S13), the data were integrated and analyzed concurrently. All samples with less than 2,000 BMMC (i.e., CD45+CD66b− singlets) after initial quality control were excluded from the supervised analysis. For unsupervised analysis, data in .fcs file format was downloaded from Cytobank. We subsequently used a workflow based on the example by Nowicka et al.[47] using the diffcyt[42] and CATALYST[41] packages in R (v3.6.1). Briefly, data was imported and transformed for analysis using the *read.flowSet()* function from the flowCore package[48] and the *prepData(…, cofactor = 5)* function from the CATALYST package respectively. Clustering was based on the FlowSOM algorithm[49] using all extracellular protein markers from

the panel on a 10 × 10 grid size with K = 20 clusters. In a first step, the clusters corresponding to CD45$^-$cells, CD66b$^+$ cells and plasma cells (i.e., clusters with expression of CD138) were removed for quality control and for consistency with the hierarchical gating approach. The remaining cells were then re-clustered using the FlowSOM algorithm using all extracellular protein markers from the panel on a 14 × 14 grid size with K = 40 clusters to create sufficient granularity and capture relevant phenotypic clusters. These clusters were visualized using heatmaps and t-distributed stochastic neighbor embedding (TSNE) dimension reduction and annotated based on canonical protein expression.

Statistical considerations

Mass cytometry data were gated to relevant populations, as shown in Figure S2. The non-parametric Mann-Whitney U-test and Wilcoxon signed-rank test were used to compare immune population frequencies in unpaired and paired analyses respectively. A two-sided p-value of less than 0.05 was considered significant. All statistical analyses were conducted in R (v3.6.1).

ADDITIONAL RESOURCES

Additional details on the clinical trial can be found at: https://clinicaltrials.gov/study/NCT02773030.

Supplemental information

Iberdomide increases innate and adaptive immune cell subsets in the bone marrow of patients with relapsed/refractory multiple myeloma

Oliver Van Oekelen, Michael Amatangelo, Manman Guo, Bhaskar Upadhyaya, Adam P. Cribbs, Geoffrey Kelly, Manishkumar Patel, Seunghee Kim-Schulze, Erin Flynt, Alessandro Lagana, Sarah Gooding, Miriam Merad, Sundar Jagganath, William E. Pierceall, Udo Oppermann, Anjan Thakurta, and Samir Parekh

Iberdomide increases innate and adaptive immune cell subsets in the bone marrow of relapsed/refractory multiple myeloma patients – SUPPLEMENTARY DATA

SUPPLEMENTARY TABLES

Table S1: Mass cytometry panel used for immune phenotyping, related to Figure 1.

T cells

CD3		Total T cells
CD4		CD4+ T cells
CD5		
CD8a		CD8+ T cells
CD25		Treg, activation
CD27		Maturation
CD28		Co-stimulatory receptor
CD38		Maturation, activation
CD45RA		Naïve/memory cells
CD56		NKT cells, T cell subsets
CD57		
CD127		T cell subsets, Treg
CD197	CCR7	Naïve/memory cells
CD226	DNAM-1	
CD274	PD-L1	Checkpoint
CD278	ICOS	Co-stimulatory receptor
CD279	PD-1	Checkpoint
Granzyme B		Cytotoxicity
HLA-DR		Activation
KLRG1		
NKG2A		
NKG2D		
T-bet		T cell subsets
TIGIT		Checkpoint
TIM-3		Checkpoint

General

CD45	Total immune cells
CD66b	Exclusion of granulocytes
CD138	Exclusion of plasma cells
Ki67	Proliferation

NK cells

CD8a	NK cell subsets
CD16	NK cell subsets
CD38	Activation
CD56	NK cell subsets
Granzyme B	Cytotoxicity
HLA-DR	Activation
NKG2A	Checkpoint
NKG2D	Activating receptor
T-bet	Maturation

Myeloid cells

CD1c		Conventional DC
CD11b		Monocytes, macrophages
CD11c		Monocytes, macrophages, DC
CD14		Monocyte subsets
CD16		Monocyte subsets
CD33		Total myeloid cells
CD123		Plasmacytoid DC
CD274	PD-L1	Checkpoint ligand
HLA-DR		Antigen presentation

B cells

CD5	B cell subsets
CD19	Total B cells
CD25	Activation
CD27	Naïve/memory cells
CD38	Naïve/memory cells
CD43	B cell subsets
HLA-DR	Antigen presentation

Table S2: mass cytometry Panel A specifications, related to Figure 1.

| Mass cytometry panel A	Vendor	Clone	Conc. (mg/mL)
Anti-human CD45 - 89Y	Fluidigm	HI30	1:100 (1µl in 100 µl staining volume)
Anti-human CD57 - 113In	Biolegend	HNK-1	0.1
Anti-human CD11c - 115In	Biolegend	BU15	0.1
Anti-human Ki67 - 141Pr	BD Biosciences	B56	0.4
Anti-human CD19 - 142Nd	Miltenyi	REA675	0.1
Anti-human CD45RA - 143Nd	Miltenyi	REA562	0.1
Anti-human KLRG1 - 144Nd	Biolegend	SA231A2	0.1
Anti-human CD4 - 145Nd	Miltenyi	REA623	0.2
Anti-human CD8 - 146Nd	Miltenyi	REA734	0.2
Anti-human ICOS - 147Sm	Biolegend	C398.4A	0.1
Anti-human CD16 - 148Nd	Miltenyi	REA423	0.4
Anti-human CD127 - 149Sm	Fluidigm	A019D5	1:100
Anti-human CD1c - 150Nd	Miltenyi	REA694	0.4
Anti-human CD123 - 151Eu	Miltenyi	REA918	0.1
Anti-human CD66b - 152Sm	Miltenyi	REA306	0.05
Anti-human TIGIT - 153Eu	Fluidigm	MBSA43	1:100
Anti-human TIM3 - 154Sm	Fluidigm	F38-2E2	1:100
Anti-human CD27 - 155Gd	Miltenyi	REA499	0.2
Anti-human PD-L1 - 156Gd	Biolegend	29E.2A3	0.4
Anti-human CD33 - 158Gd	Fluidigm	WM53	1:100
Anti-human CD138 - 159Tb	Biolegend	MI15	0.4
Anti-human CD14 - 160Gd	Miltenyi	REA599	0.1
Anti-human CD56 - 161Dy	Miltenyi	REA196	0.5
Anti-human NKG2A - 162Dy	Miltenyi	REA110	0.1
Anti-human CD5 - 163Dy	Biolegend	UCHT2	0.1
Anti-human CD43 - 164Dy	Biolegend	CD43-10G7	0.4
Anti-human NKG2D - 165Ho	Biolegend	1D11	0.2
Anti-human CD25 - 166Er	Miltenyi	REA570	0.2
Anti-human CCR7 - 167Er	Fluidigm	G043H7	1:100
Anti-human CD3 - 168Er	Miltenyi	REA613	0.1
Anti-human Tbet - 169Tm	Biolegend	4B10	0.2
Anti-human CD38 - 170Er	Miltenyi	REA671	0.1
Anti-human CXCR3 - 171Yb	Miltenyi	REA232	0.2
Anti-human CD28 - 172Yb	Biolegend	CD28.2	0.1
Anti-human CD226 - 173Yb	Biolegend	11A8	0.1
Anti-human HLA-DR - 174Yb	Miltenyi	REA805	0.05
Anti-human PD-1 - 175Lu	Fluidigm	EH12.2H7	1:100
Anti-human GranzymeB - 176Yb	Miltenyi	REA226	0.1
Anti-human CD11b - 209Bi	Fluidigm	ICRF44	1:100

Table S3: high-level annotation of 40 unsupervised clusters shown in Supplementary Figure 1C, related to Figure 1.

original_cluster	new_cluster
1	MYELOID/MONOCYTE
2	MYELOID/MONOCYTE
3	OTHER/MULTIPLET
4	MYELOID/MONOCYTE
5	NK CELL
6	NK CELL
7	NK CELL
8	NKT CELL
9	MYELOID/MONOCYTE
10	MYELOID/MONOCYTE
11	NK CELL
12	MYELOID/MONOCYTE
13	OTHER/MULTIPLET
14	OTHER/MULTIPLET
15	MYELOID/MONOCYTE
16	MYELOID/MONOCYTE
17	OTHER/MULTIPLET
18	T CELL CD8
19	MYELOID/MONOCYTE
20	MYELOID/MONOCYTE
21	MYELOID/MONOCYTE
22	MYELOID/MONOCYTE
23	MYELOID/MONOCYTE
24	OTHER/MULTIPLET
25	T CELL DN
26	MYELOID/MONOCYTE
27	OTHER/MULTIPLET
28	OTHER/MULTIPLET
29	T CELL CD8
30	MYELOID/MONOCYTE
31	pDC
32	NKT CELL
33	pDC
34	OTHER/MULTIPLET
35	T CELL CD4
36	T CELL DP
37	OTHER/MULTIPLET
38	B CELL
39	NKT CELL
40	OTHER/MULTIPLET

SUPPLEMENTARY FIGURES AND FIGURE LEGENDS

SUPPLEMENTARY FIGURE 1

Figure S1: Unsupervised gating strategy supports manual gating findings, related to Figure 1. (A) Heatmap showing normalized protein expression of the (n=39) protein markers included in the custom mass cytometry (CyTOF) panel developed for this study across the manually annotated clusters. Population abbreviations are as follows (with associated characteristic phenotypic marker expression): T CELL DN = double negative T cell (i.e., CD4-/CD8-/CD3+), NKT CELL = natural killer T cell (i.e., CD4+ or CD8+, CD3+CD56+), T CELL CD8 EM/EFF = effector(-memory) CD8+ T cell (i.e., CD3+CD8+CCR7-), T CELL CD4 = CD4+ T cell (i.e., CD3+CD4+), T CELL CD8 N = naïve/central-memory CD8+ T cell (i.e., CD3+CD8+CCR7+), T CELL DP = double positive T cell (i.e., CD4+/CD8+/CD3+), NK CELL = natural killer cell (i.e., CD3-CD56+), cDC = conventional dendritic cell (i.e. CD11c+CD1c+), MONOCYTE = monocyte/macrophage (i.e., CD11b+ CD14+ or CD16+), B CELL = B cell (i.e., CD19+), pDC = plasmacytoid dendritic cell (i.e., CD123+). **(B)** Protein expression of canonical markers used for cell type annotation, including CD3, CD4 and CD8 (T cells), CD19 (B cells), CD56 (natural killer cells), CD11b (monocytes) and CD123 (plasmacytoid dendritic cells). Expression is show on a normalized scale from low (blue) to high (red) expression. **(C)** Heatmap illustrating the 40 unsupervised cluster of immune cell subsets generated by the 2-step FlowSOM methods (see Methods). The 40 clusters were given high level annotation as shown in **Table S3** that was used for exploratory data analysis.

A
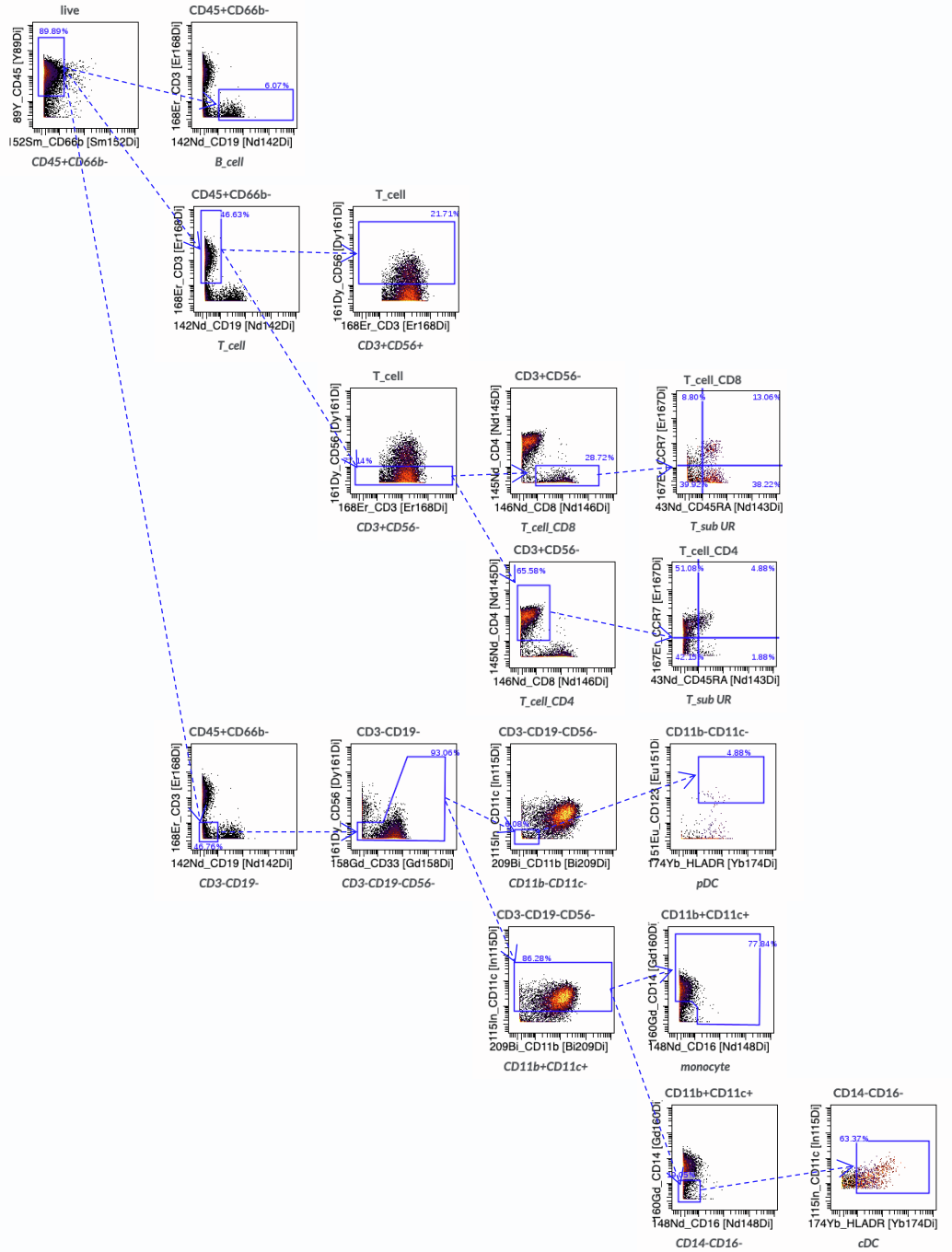
SUPPLEMENTARY FIGURE 2

Figure S2: Manual hierarchical gating strategy of detailed immune cell phenotypes, related to Figures 1-5.

(A) Bivariate plots showing the manual hierarchical gating strategy used on human bone marrow mononuclear cells (BMMC) measured by mass cytometry. Intact live cells were defined using iridium-based cell markers and the rhodium viability stain. BMMC were defined as CD45+CD66b- events. CD3, CD11b, CD11c, CD14, CD16, CD19, CD56, CD123 and HLA-DR were used to identify B cells, T cells, NK(T) cells, monocytes, and dendritic cells. T cells were differentiated based on expression of CD45RA and CCR7 as shown. Within each of these population expression of activation/exhaustion markers was determined.

A

SUPPLEMENTARY FIGURE 3
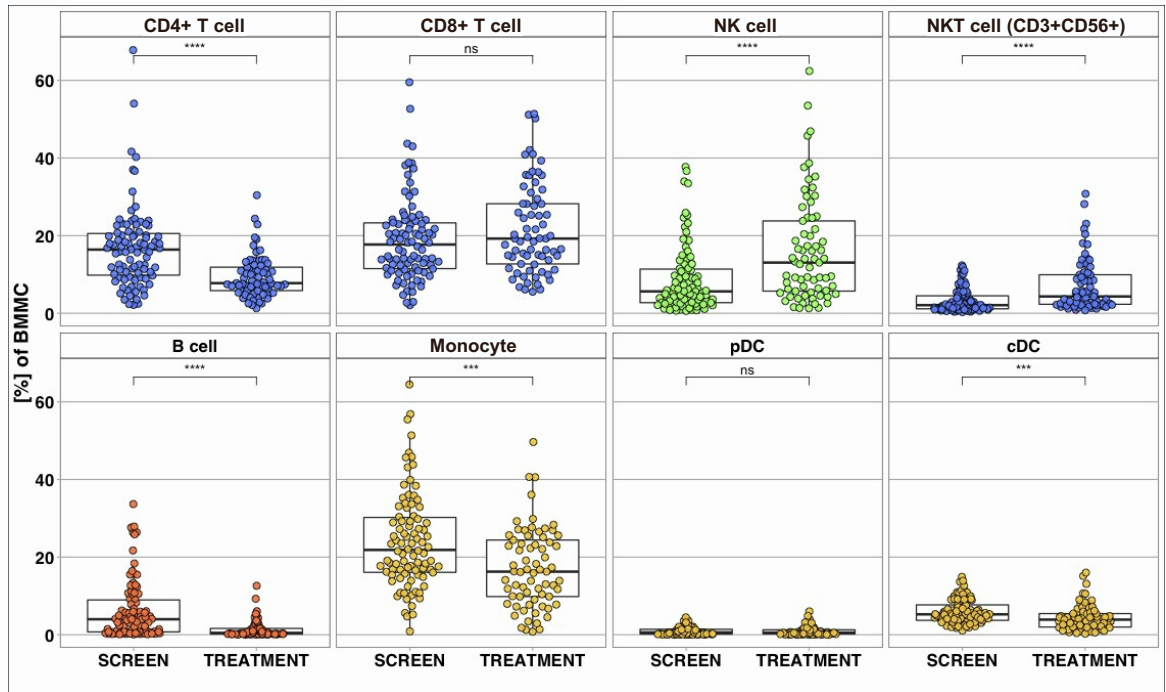
Figure S3: Iberdomide induces expansion of NK and NKT cells in the bone marrow microenvironment of relapsed/refractory multiple myeloma patients, related to Figure 1. (A) Relative abundances of major immune cell populations (CD4+ T cells, CD8+ T cells, natural killer (NK) cells, NKT cells, B cells, monocytes, plasmacytoid dendritic cells (pDC) and conventional dendritic cells (cDC)) as a percentage of bone marrow mononuclear cells (BMMC), shown before treatment with iberdomide ± dexamethasone (SCREEN) and at the cycle 2 day 15 timepoint (TREATMENT). Each dot represents a patient sample. Box plots show median, Q1 and Q3 quartiles and whiskers up to 1.5x interquartile range (****, p<0.0001; ***, p<0.001; **, p<0.01; *, p<0.05; ns, p≥0.05, Mann-Whitney *U* test).

A
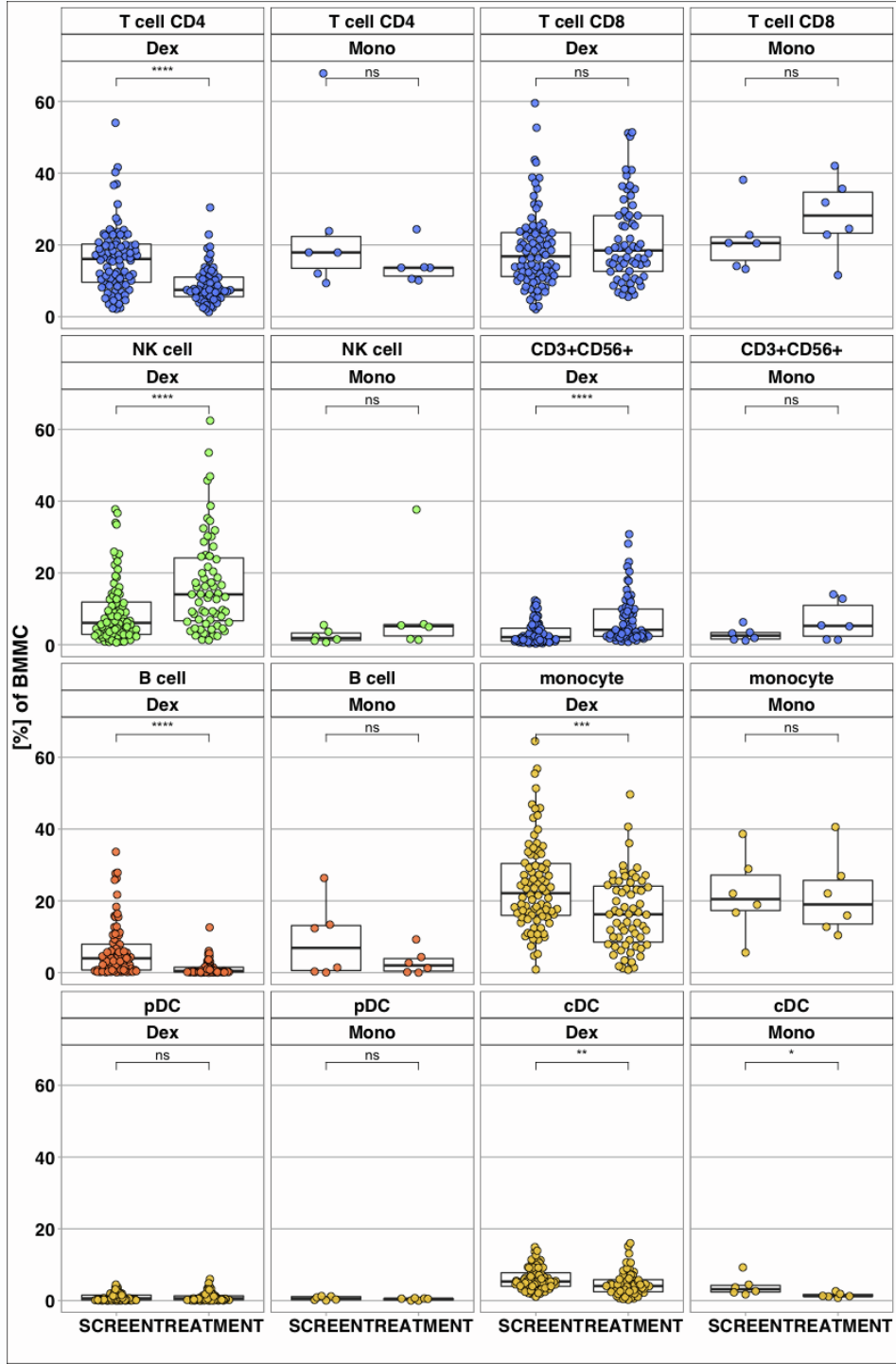
SUPPLEMENTARY FIGURE 4

Figure S4: Changes induced by iberdomide monotherapy are comparable to the changes observed in patients treated with iberdomide in combination with dexamethasone, related to Figure 1. (A) Relative abundances of major immune cell populations (CD4+ T cells, CD8+ T cells, natural killer (NK) cells, NKT cells, B cells, monocytes, plasmacytoid dendritic cells (pDC) and conventional dendritic cells (cDC)) as a percentage of bone marrow mononuclear cells (BMMC), shown before treatment with iberdomide ± dexamethasone (SCREEN) and at the cycle 2 day 15 timepoint (TREATMENT). Data are shown for patients treated with iberdomide in combination with dexamethasone (Dex) and for patients treated with iberdomide monotherapy (Mono). Each dot represents a patient sample. Box plots show median, Q1 and Q3 quartiles and whiskers up to 1.5x interquartile range (****, $p < 0.0001$; ***, $p < 0.001$; **, $p < 0.01$; *, $p < 0.05$; ns, $p \geq 0.05$, Mann-Whitney U test).
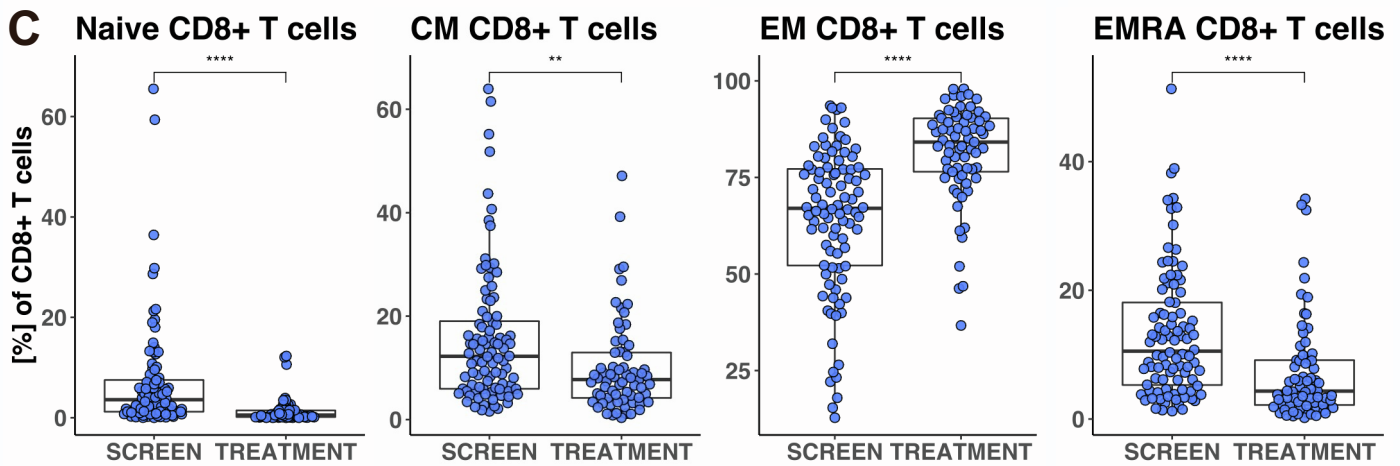
A

CD4+ NKT cells   **CD8+ NKT cells**

B

Naive CD4+ T cells   **CM CD4+ T cells**   **EM CD4+ T cells**   **EMRA CD4+ T cells**

C

Naive CD8+ T cells   **CM CD8+ T cells**   **EM CD8+ T cells**   **EMRA CD8+ T cells**
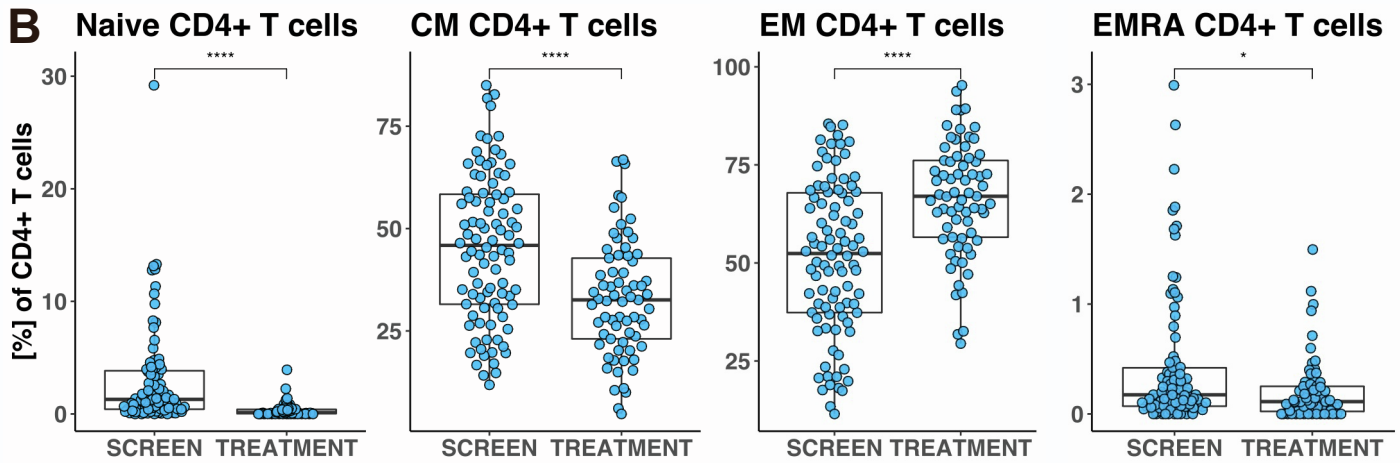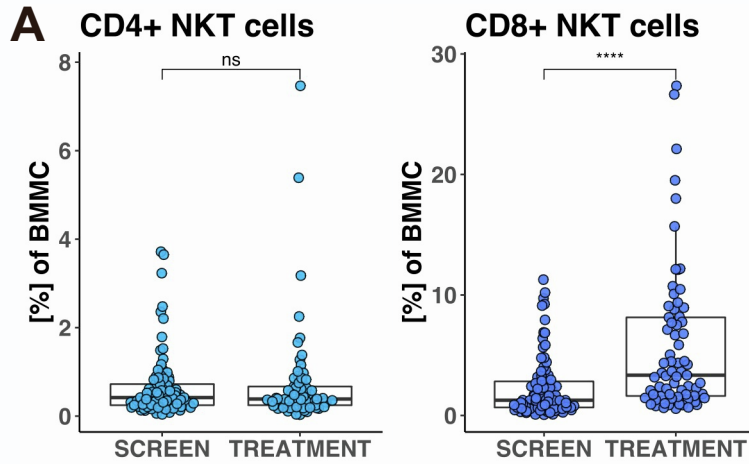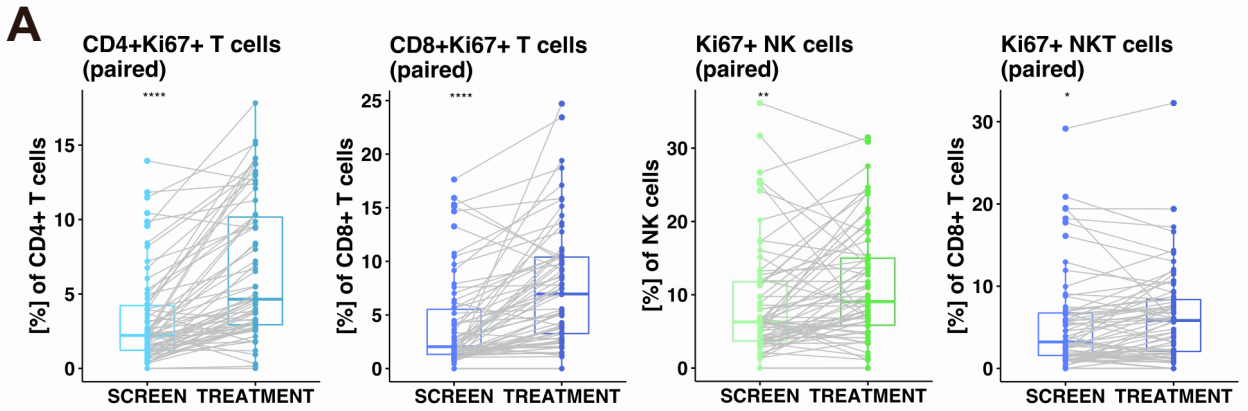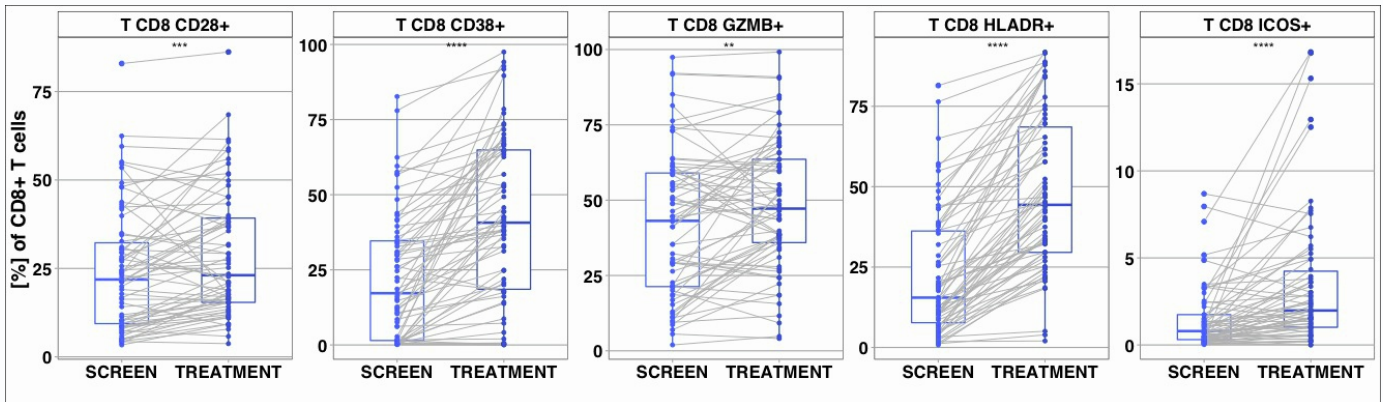
SUPPLEMENTARY FIGURE 5

Figure S5: Mid-cycle 2 changes (cycle 2 day 15) of T cell differentiation following iberdomide treatment, related to Figures 1-3. (A) Relative abundances of CD4+ or CD8+ natural killer T (NKT) cells as a percentage of bone marrow mononuclear cells (BMMC) before treatment with iberdomide ± dexamethasone (SCREEN) and at the cycle 2 day 15 timepoint (TREATMENT). **(B-C)** Relative abundance of CD4+ **(B)** and CD8+ **(C)** T cell subsets as a percentage of all CD4+ **(B)** and CD8+ **(C)** T cells (parent population) before treatment with iberdomide ± dexamethasone (SCREEN) and at the cycle 2 day 15 timepoint (TREATMENT). T cell differentiation subsets were defined based on the expression of CCR7 and CD45RA and included naïve (N, CCR7+CD45RA+), central-memory (CM, CCR7+CD45RA-), effector-memory (EM, CCR7-CD45RA-) and terminally differentiated effector-memory cells re-expressing CD45RA (EMRA, CCR7-CD45RA+). In panels **(A-C)**, each dot represents a patient sample. Box plots show median, Q1 and Q3 quartiles and whiskers up to 1.5x interquartile range (****, $p<0.0001$; ***, $p<0.001$; **, $p<0.01$; *, $p<0.05$; ns, $p\geq0.05$, Mann-Whitney U test).

A CD4+Ki67+ T cells (paired) — CD8+Ki67+ T cells (paired) — Ki67+ NK cells (paired) — Ki67+ NKT cells (paired)

B T cell activation markers

T CD8 CD28+ — T CD8 CD38+ — T CD8 GZMB+ — T CD8 HLADR+ — T CD8 ICOS+

C T cell exhaustion / immune checkpoint markers

T CD8 CD57+ — T CD8 KLRG1+ — T CD8 PD1+ — T CD8 TIGIT+ — T CD8 KLRG1+PD1+TIGIT+

SUPPLEMENTARY FIGURE 6
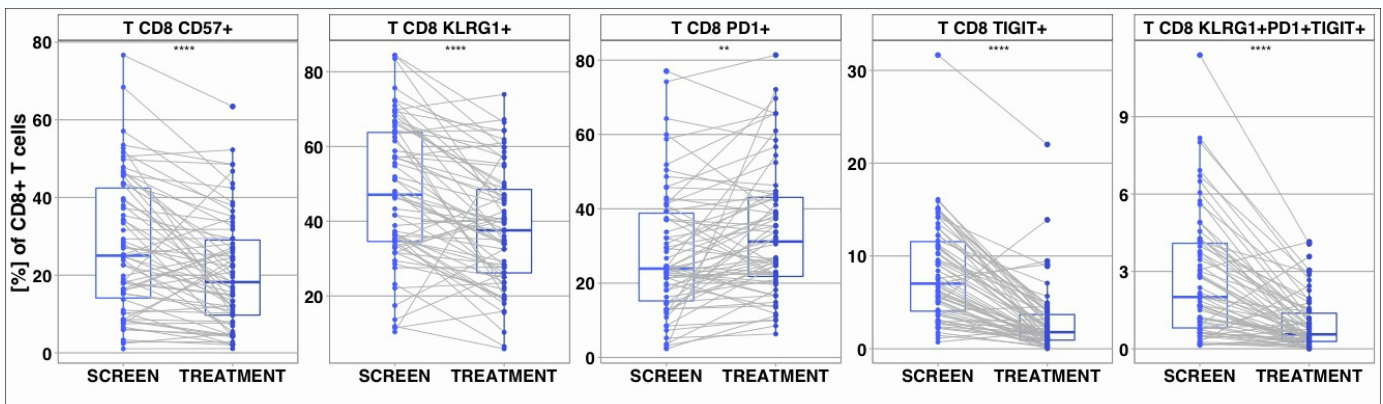
Figure S6: Mid-cycle 2 changes (cycle 2 day 15) of the immune phenotype following iberdomide treatment show activation/proliferation of T and NK cells, related to Figures 2-4. (A) Relative abundance of the Ki-67+ population as a percentage of all CD4+ T cells, CD8+ T cells, NK cells or NKT cells respectively, shown before treatment with iberdomide ± dexamethasone (SCREEN) and at the cycle 2 day 15 timepoint (TREATMENT). **(B)** Relative abundances of CD8+ T cells expressing the activation markers shown as a percentage of all CD8+ T cells (parent population) within paired samples, shown before treatment with iberdomide ± dexamethasone (SCREEN) and at the cycle 2 day 15 timepoint (TREATMENT). **(C)** Relative abundances of CD8+ T cells expressing the exhaustion/immune checkpoint markers shown as a percentage of all CD8+ T cells (parent population) within paired samples, shown before treatment with iberdomide ± dexamethasone (SCREEN) and at the cycle 2 day 15 timepoint (TREATMENT). In panels **(A-C)**, each dot represents a patient sample. Box plots show median, Q1 and Q3 quartiles and whiskers up to 1.5x interquartile range (****, $p<0.0001$; ***, $p<0.001$; **, $p<0.01$; *, $p<0.05$; ns, $p≥0.05$, paired Mann-Whitney U test).
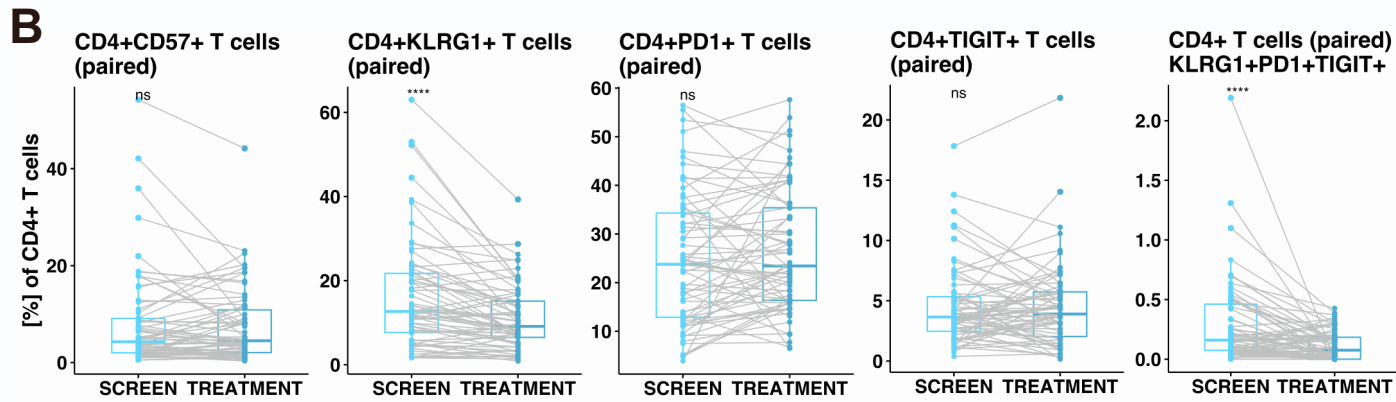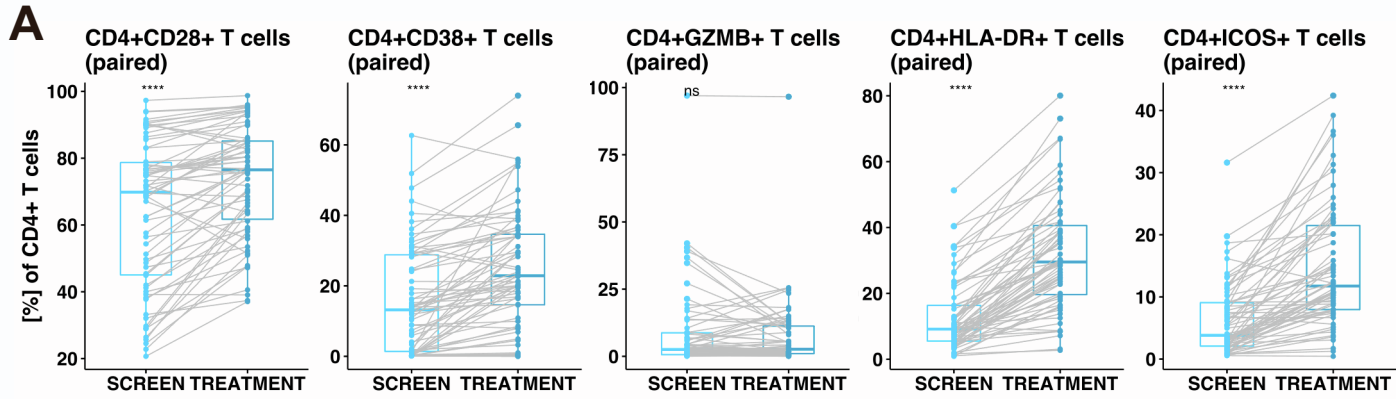
A

CD4+CD28+ T cells (paired) ****

CD4+CD38+ T cells (paired) ****

CD4+GZMB+ T cells (paired) ns

CD4+HLA-DR+ T cells (paired) ****

CD4+ICOS+ T cells (paired) ****

B

CD4+CD57+ T cells (paired) ns

CD4+KLRG1+ T cells (paired) ****

CD4+PD1+ T cells (paired) ns

CD4+TIGIT+ T cells (paired) ns

CD4+ T cells (paired) KLRG1+PD1+TIGIT+ ****

[%] of CD4+ T cells

SCREEN TREATMENT

SUPPLEMENTARY FIGURE 7

Figure S7: Mid-cycle 2 changes (cycle 2 day 15) of the immune phenotype in CD4+ T cells, related to Figures 1-3. (A) Relative abundances of CD4+ T cells expressing the activation markers as shown as a percentage of all CD4+ T cells (parent population) within paired samples, shown before treatment with iberdomide ± dexamethasone (SCREEN) and at the cycle 2 day 15 timepoint (TREATMENT). **(B)** Relative abundances of CD4+ T cells expressing the exhaustion/immune checkpoint markers as shown as a percentage of all CD4+ T cells (parent population) within paired samples, shown before treatment with iberdomide ± dexamethasone (SCREEN) and at the cycle 2 day 15 timepoint (TREATMENT). In panels **(A-B)**, each dot represents a patient sample. Box plots show median, Q1 and Q3 quartiles and whiskers up to 1.5x interquartile range (****, p<0.0001; ***, p<0.001; **, p<0.01; *, p<0.05; ns, p≥0.05, paired Mann-Whitney *U* test).

A B cells

B NK cells

C CD8+HLADR+ T cells

D CD8+TIGIT+ T cells

E Monocytes

F cDC

G CD8+Ki67+ T cells

H CD8+KLRG1+ T cells

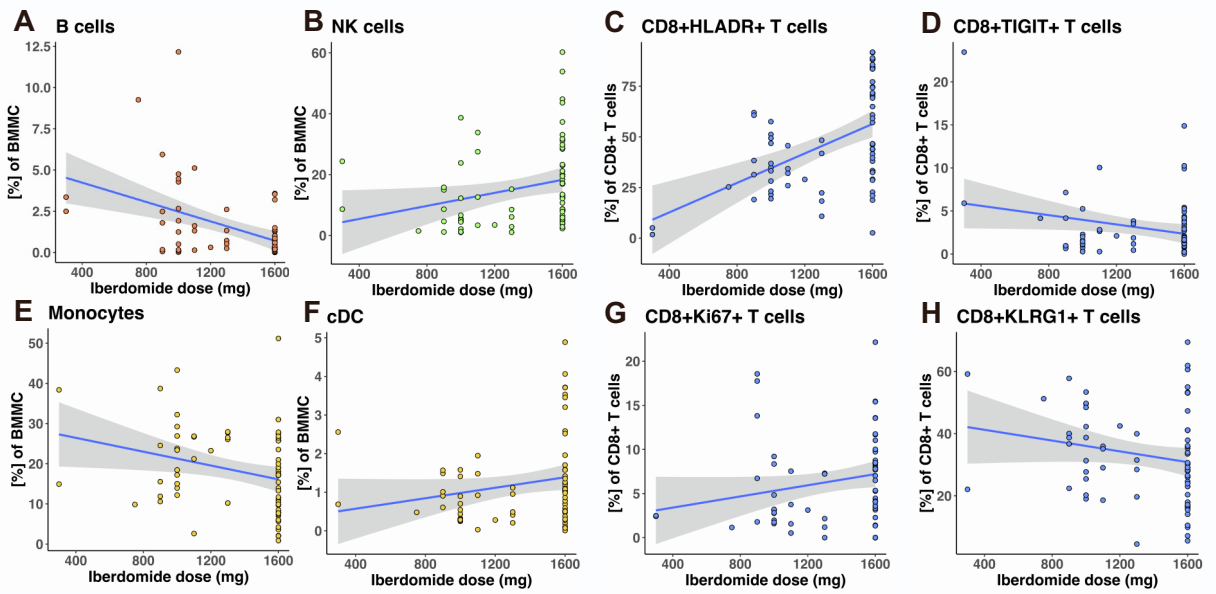**SUPPLEMENTARY FIGURE 8**

Figure S8: Shifts in the immune phenotypic composition correlate with iberdomide dose, related to Figures 1-2. (A-H) Relative abundances of selected immune cell populations as a percentage of bone marrow mononuclear cells (BMMC) **(A-D)** or all CD8+ T cells **(E-H)** plotted against the iberdomide dose within samples collected at the cycle 2 day 15 timepoint. Each dot represents a patient sample. Regression lines shown represent the best fitting linear model with 95% confidence interval shown as the shaded region.

A
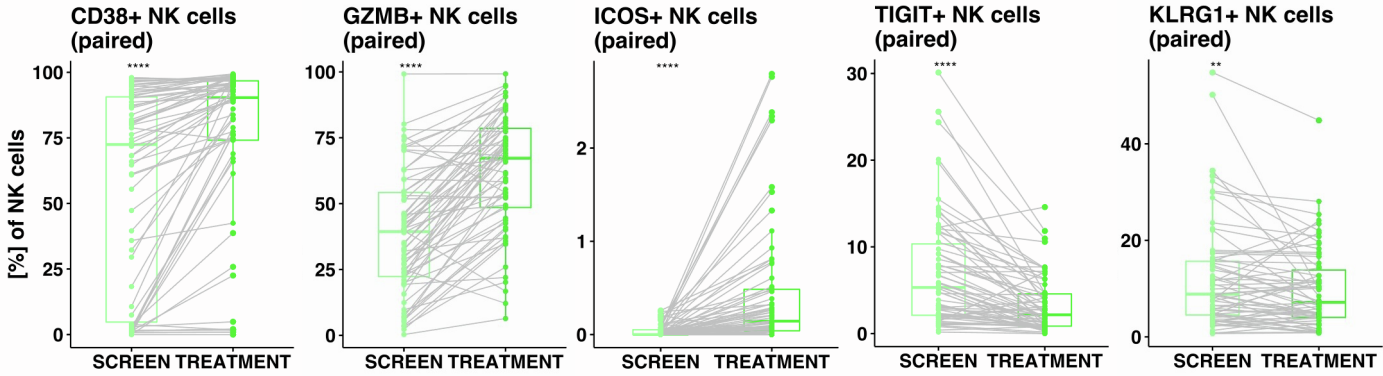
NK cell markers

SUPPLEMENTARY FIGURE 9
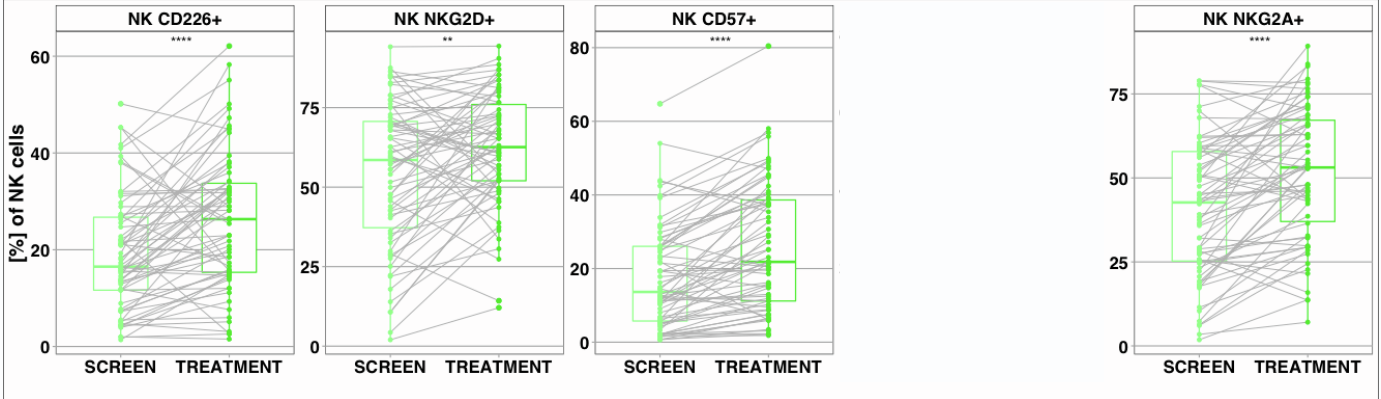
Figure S9: Mid-cycle 2 changes (cycle 2 day 15) of the immune phenotype in NK cells, related to Figure 4. (A) Relative abundances of natural killer (NK) cells expressing the markers as shown as a percentage of all NK cells (parent population) within paired samples, shown before treatment with iberdomide ± dexamethasone (SCREEN) and at the cycle 2 day 15 timepoint (TREATMENT). Each dot represents a patient sample. Box plots show median, Q1 and Q3 quartiles and whiskers up to 1.5x interquartile range (****, p<0.0001; ***, p<0.001; **, p<0.01; *, p<0.05; ns, p≥0.05, paired Mann-Whitney U test).
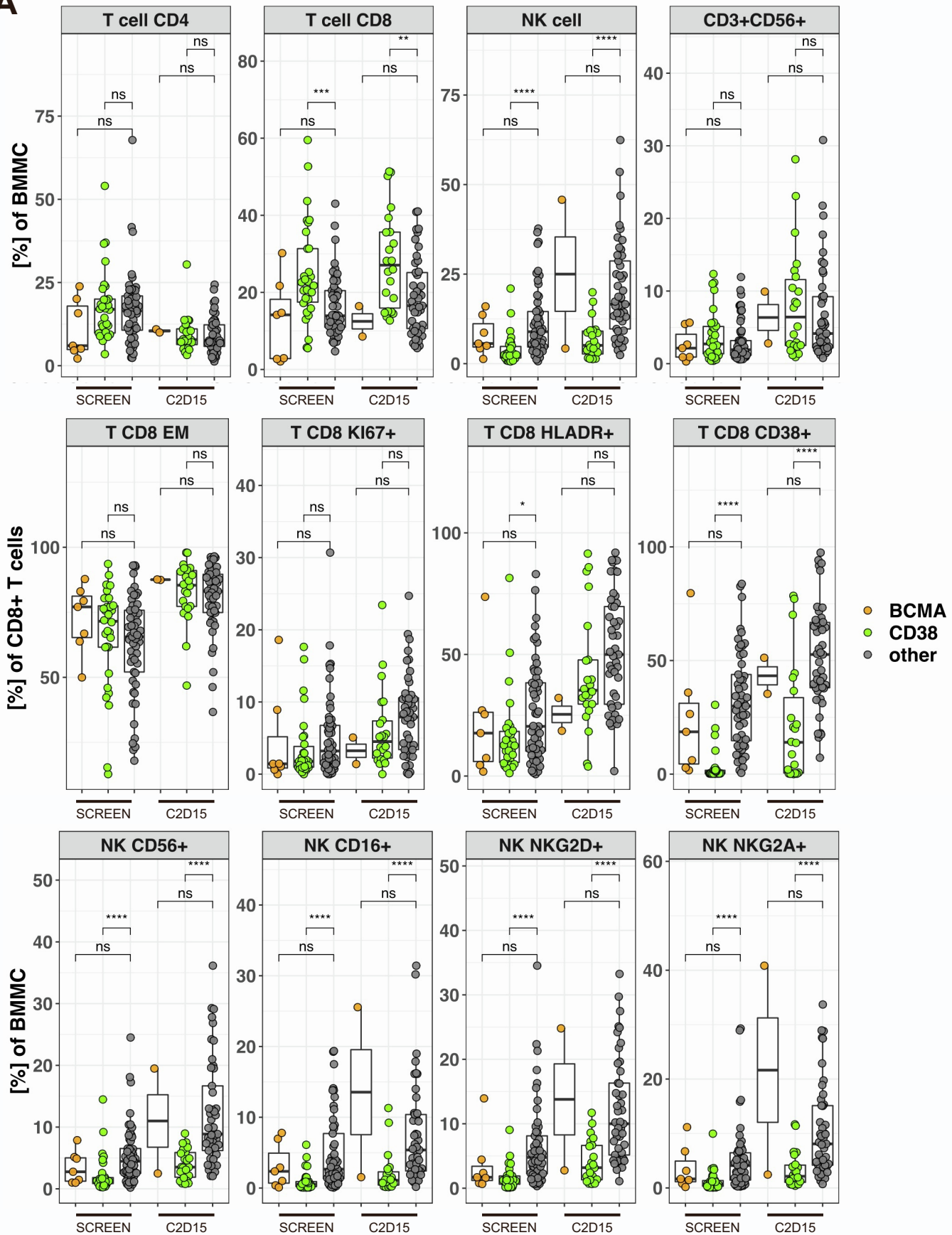
SUPPLEMENTARY FIGURE 10

Figure S10: Immediate prior therapy regimen variability is associated with differential composition of the immune microenvironment of RRMM patients prior to iberdomide therapy, related to Figure 5. (A) Relative abundance of selected T/NK/NKT cell populations within samples, shown before treatment with iberdomide ± dexamethasone (SCREEN) and at the cycle 2 day 15 timepoint (TREATMENT). Subjects are split by the last prior therapy before enrollment on the study: BCMA-targeted therapy (orange), anti-CD38 monoclonal antibody (green) or all other (gray). In panel **(A)**, each dot represents a patient sample. Box plots show median, Q1 and Q3 quartiles and whiskers up to 1.5x interquartile range (****, $p<0.0001$; ***, $p<0.001$; **, $p<0.01$; *, $p<0.05$; ns, $p \geq 0.05$, Mann-Whitney U test).
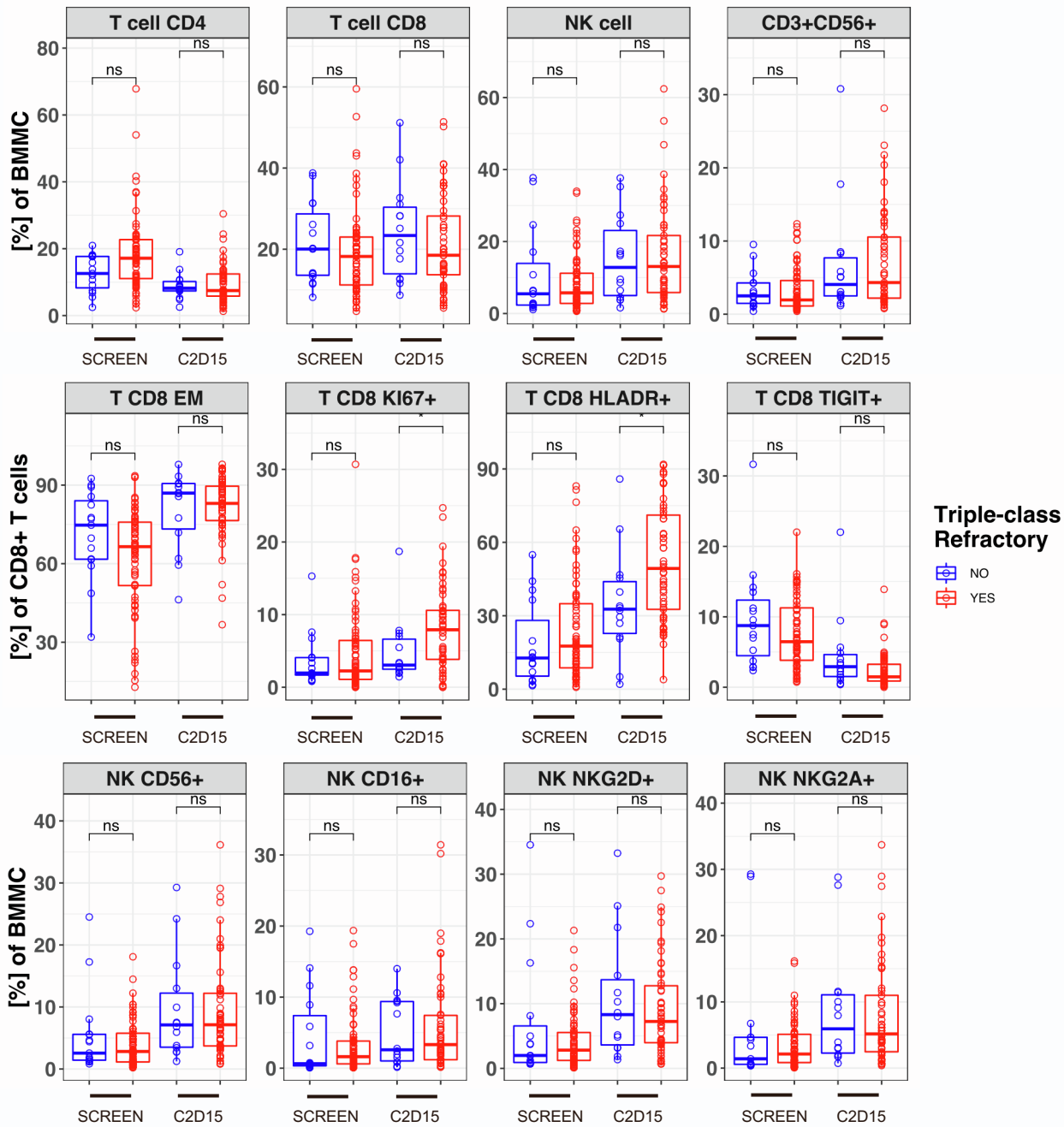
A

SUPPLEMENTARY FIGURE 11

Figure S11: Association of immune phenotype and immunomodulatory changes after iberdomide treatment to prior treatment refractoriness, related to Figure 5. (A) Relative abundance of selected T/NK/NKT cell populations within samples, shown before treatment with iberdomide ± dexamethasone (SCREEN) and at the cycle 2 day 15 timepoint (TREATMENT). Subjects are split based on triple-class refractory status, defined as refractory to ≥1 immunomodulatory drug, ≥1 proteasome inhibitor, and ≥1 CD38 monoclonal antibody. In panel **(A)**, each dot represents a patient sample. Box plots show median, Q1 and Q3 quartiles and whiskers up to 1.5x interquartile range (****, $p<0.0001$; ***, $p<0.001$; **, $p<0.01$; *, $p<0.05$; ns, $p\geq0.05$, Mann-Whitney U test).

A B-cells (CD3-CD19+)
p < 0.0001

B T-cells (CD3+)

C NK Cells (CD3-CD56+/CD16+)

D Monocytes (CD14+)
p < 0.0001

E NK Cells (CD3-CD56+/CD16+)
p < 0.0001

F T-cells (CD3+)
p < 0.0001

G T-cells (CD3+CD8+)
p < 0.0001

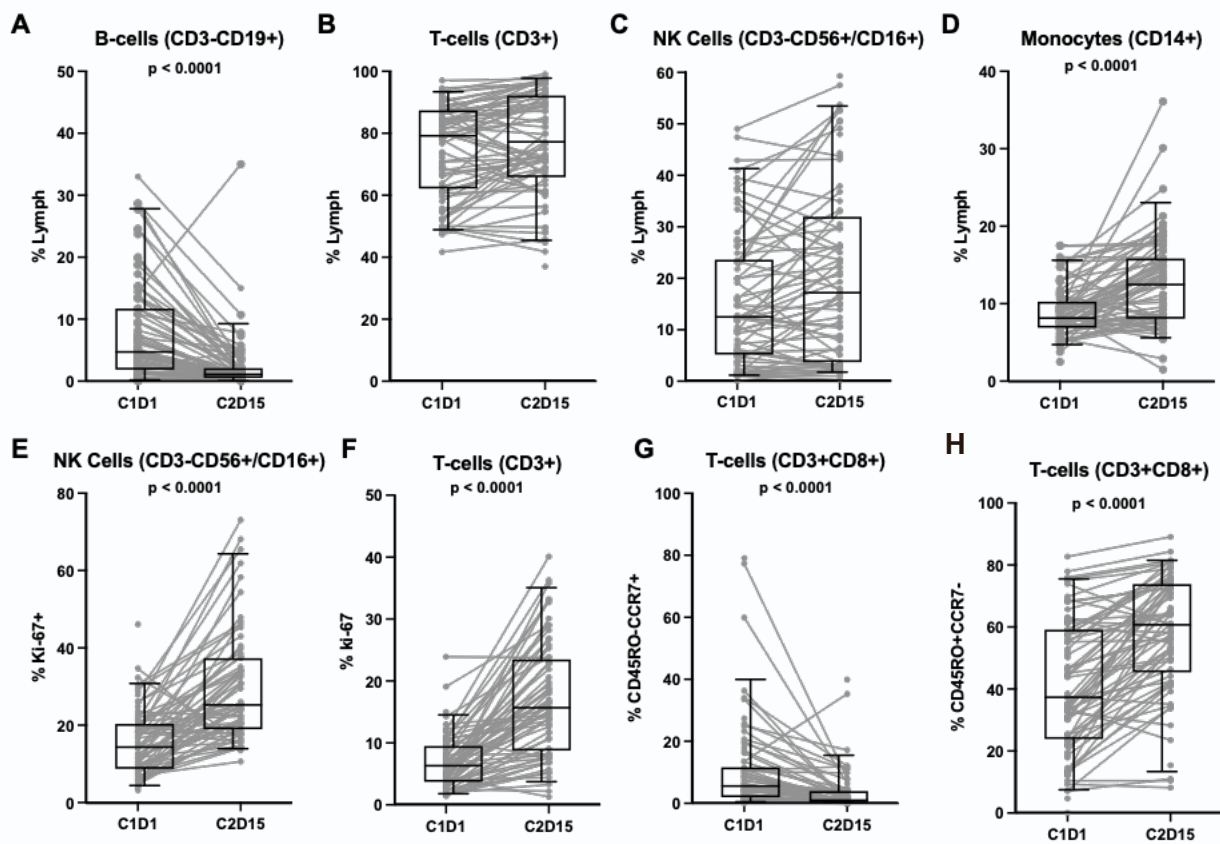**H** T-cells (CD3+CD8+)
p < 0.0001

SUPPLEMENTARY FIGURE 12

Figure S12: Peripheral blood phenotyping studies support systemic proliferation and activation of immune cell subsets as shown in the tumor microenvironment, related to Figures 1-2. (A-D) Relative abundance of **(A)** B cells (CD3-CD19+), **(B)** T cells (CD3+), **(C)** natural killer (NK) cells (CD3-CD56+/CD16+) and **(D)** monocytes (CD14+) as a percentage of total lymphocytes before treatment with iberdomide ± dexamethasone (C1D1) and at the cycle 2 day 15 timepoint (C2D15) in the peripheral blood. **(E-F)** Relative abundance of the Ki-67+ population as a percentage of all NK cells **(E)** and T cells **(F)** respectively, shown before treatment with iberdomide ± dexamethasone (C1D1) and at the cycle 2 day 15 timepoint (C2D15) in the peripheral blood. **(G-H)** Relative abundance of CCR7+CD45RO- (naïve) CD8+ T cells **(G)** and CCR7-CD45RO+ (effector-memory) CD8+ T cells **(H)** as a percentage of all CD8+ T cells, shown before treatment with iberdomide ± dexamethasone (C1D1) and at the cycle 2 day 15 timepoint (C2D15) in the peripheral blood. In panels **(A-H)**, each dot represents a patient sample. Box plots show median, Q1 and Q3 quartiles and whiskers up to 1.5x interquartile range (****, $p < 0.0001$; ***, $p < 0.001$; **, $p < 0.01$; *, $p < 0.05$; ns, $p \geq 0.05$, Mann-Whitney U test).
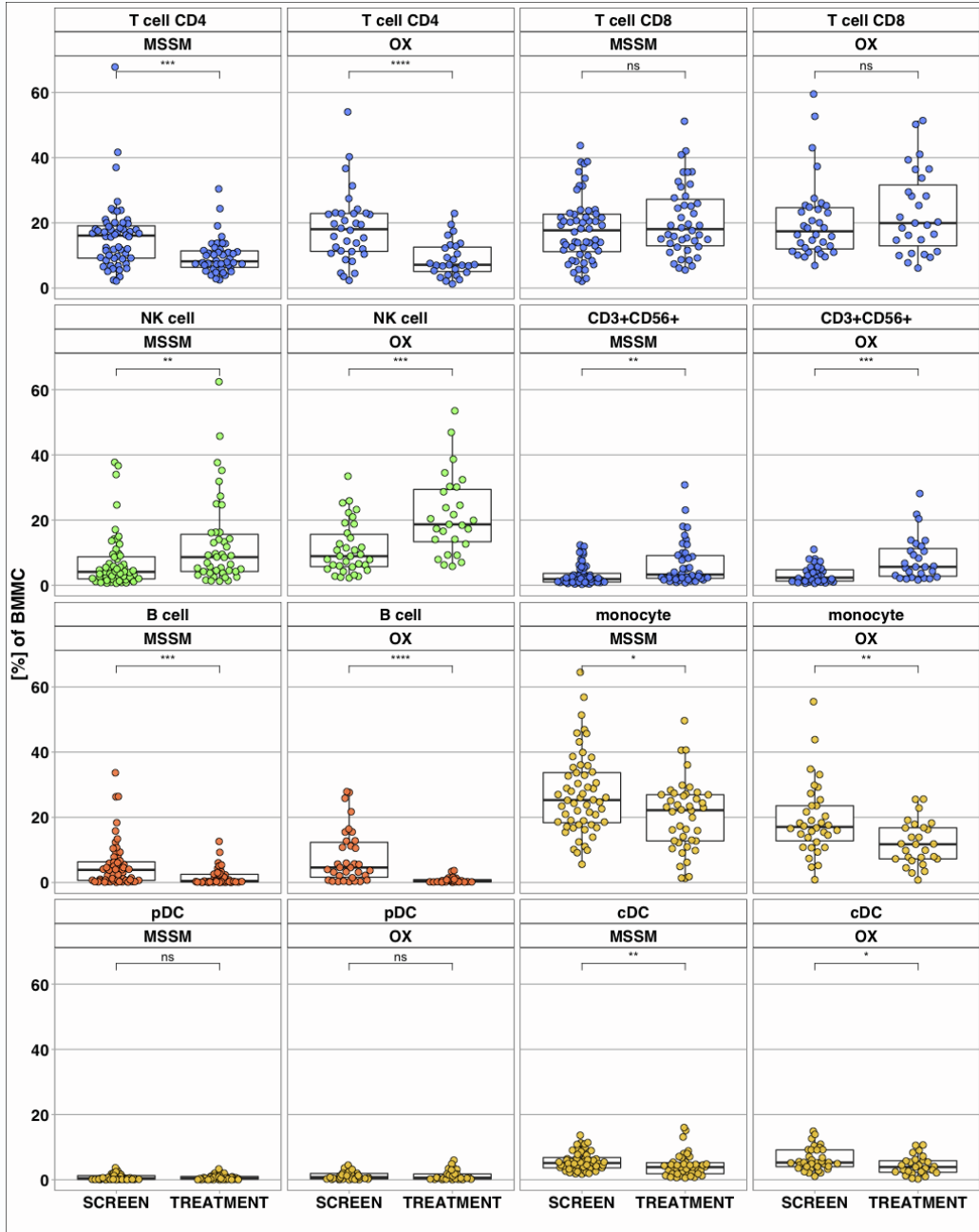
A

SUPPLEMENTARY FIGURE 13

Figure S13: Changes in major immune cell populations are comparable between the 2 processing sites, related to Figure 1. (A) Relative abundances of major immune cell populations (CD4+ T cells, CD8+ T cells, natural killer (NK) cells, NKT cells, B cells, monocytes, plasmacytoid dendritic cells (pDC) and conventional dendritic cells (cDC)) as a percentage of bone marrow mononuclear cells (BMMC), shown before treatment with iberdomide ± dexamethasone (SCREEN) and at the cycle 2 day 15 timepoint (TREATMENT). Data are shown for patient samples processed in the United States (MSSM) and for samples processed in Europe (OX). Each dot represents a patient sample. Box plots show median, Q1 and Q3 quartiles and whiskers up to 1.5x interquartile range (****, p<0.0001; ***, p<0.001; **, p<0.01; *, p<0.05; ns, p≥0.05, Mann-Whitney U test).